Post-Print

This is the accepted version of:

Robust Stability Analysis of Adverse Aeroelastic Roll/Lateral Rotorcraft-Pilot Couplings

Vincenzo Muscarello, Pierangelo Masarati, Giuseppe Quaranta*

Dept. of Aerospace Science and Technology, Politecnico di Milano,

Milano, Italy

Abstract

This paper investigates the roll/lateral rotorcraft-pilot coupling, a phenomenon caused by the interaction between the pilot's involuntary biodynamic response on the cyclic stick and the aeroelastic response of the helicopter. Such interaction falls under a class of events, denominated pilot augmented oscillations, that may significantly affect helicopters. This phenomenon was experienced during an piloted flight simulation campaign performed in a flight simulator. An analytical model of the coupled rotorcraft-pilot problem is developed and validated. This model is used to understand the physics that govern this instability, and the most influential parameters. The model is subsequently used to perform several sensitivity analyses with respect to basic helicopter design parameters. The stability of helicopters with soft-inplane hingeless main rotor design showed significant sensitivity to the amount of damping in the regressive lead-lag mode. Such mode may interact with the pilot since it can transmit lateral vibrations to the airframe in the vicinity of the pilot's fundamental biodynamic feedthrough frequency. Furthermore, it is shown that an increase in main rotor loading may reduce the stability margins. The results of the sensitivity analysis give the rotorcraft designer the capability to infer how rotor design may be prone to rotorcraft-pilot coupling and what mitigation actions can be taken.

---

*Corresponding author.

Nomenclature

a_Y^{seat}	=	Lateral acceleration at the pilot's seat, g
$\mathbf{B}\,(\mathbf{p})$	=	Input matrix of the helicopter model
C_b	=	Lead-lag viscous damping, N·m·s·rad^{-1}
C_T	=	Thrust coefficient
C_{XY}	=	Cross-coupling cyclic stick parameter
$\mathbf{C}\,(\mathbf{p})$	=	Damping matrix of the helicopter model
$\mathbf{D}$	=	Output matrix of the helicopter model
G_{1C}, G_{1S}	=	Gearing ratios between stick displacement and blade cyclic pitch rotation, deg/%
G_Y	=	Loop transfer function gain
$H_{\text{PP}}\,(s)$	=	Pilot-lateral stick dynamic transfer function, %/g
$H_{\text{YC}}\,(s, \mathbf{p}), H_{\text{YS}}\,(s, \mathbf{p})$	=	Helicopter transfer functions, m·s^{-2}·rad^{-1}
$H_{nom}\,(s, \mathbf{p})$	=	Nominal loop transfer function
I_{xx}, I_{yy}	=	Helicopter roll and pitch moment of inertia, kg·m^2
K_{p_β}, K_{p_ζ}	=	Pitch-flap and pitch-lag kinematic couplings
$\mathbf{K}\,(\mathbf{p})$	=	Stiffness matrix of the helicopter model
$\mathbf{M}\,(\mathbf{p})$	=	Mass matrix of the helicopter model
$\mathbf{p}$	=	Vector of trim parameters of the helicopter model
$\mathbf{q}$	=	State vector of the helicopter model
R	=	Rotor radius, m
T_p	=	Pilot-lateral stick model real pole time constant, s
T_z	=	Pilot-lateral stick model zero time constant, s
$\mathbf{u}$	=	Input vector of the helicopter model
y	=	Output of the helicopter model
$(\hat{\cdot})$	=	Value at the stability boundary
$(\cdot)'$	=	Derivative to respect the azimuthal coordinate
$\Im(\cdot)$	=	Imaginary part
$\Re(\cdot)$	=	Real part

α_X, α_Y =   Airframe roll and pitch angles

β_{1C}, β_{1S} =   Cyclic rotor flap modes

ζ_{1C}, ζ_{1S} =   Cyclic rotor lead-lag modes

$\vartheta_{1C}, \vartheta_{1S}$ =   Cyclic rotor pitch modes

δ_X, δ_Y =   Longitudinal and lateral stick displacement, %

γ =   Main rotor Lock number

σ =   Main rotor solidity

β_0 =   Main rotor coning angle, rad

ϑ_0 =   Collective pitch angle, rad

ν_β =   Non-dimensional rotating natural frequency of blade flap mode

ν_ζ =   Non-dimensional rotating natural frequency of blade lead-lag mode

ν_ϑ =   Non-dimensional rotating natural frequency of blade pitch mode

μ_P =   Pilot-lateral stick model gain, %/g

ξ =   Pilot-lateral stick model complex poles damping factor

ω_n =   Pilot-lateral stick model complex poles frequency, rad/s

τ_Y =   Loop transfer function time delay, s

ψ =   Azimuthal coordinate, rad

Ω =   Rotor angular velocity, rad/s

Introduction

Adverse interactions between aircraft and pilot dynamics fall under the definition of Aircraft-Pilot Couplings (APCs, Ref. 1), or Rotorcraft-Pilot Couplings (RPCs, Ref. 2) when specifically referred to rotary wing aircraft. These phenomena occur when the pilot introduces an inadvertent or unintentional command in the control system as a consequence of the vehicle dynamics, resulting in oscillatory or divergent motions, difficulty in performing the desired tasks and, ultimately, loss of control.

The interaction between the pilot and the vehicle can be of two kinds. The first, called Pilot-Induced

Oscillations (PIO), is the result of the intentional application of erroneous controls, often as a consequence of insufficient or misleading cues. Since there are inherent limitations of the human operator's bandwidth, interactions of this kind occur with the low frequency dynamics of the vehicle, thus specifically affecting the flight mechanics modes, or in any case dynamics whose characteristic frequencies fall below 1 Hz (Ref. 3).

The second kind, called Pilot-Assisted Oscillations or Pilot-Augmented Oscillations (PAO), is the result of the unintentional application of controls caused by vibrations of the cockpit. In this case, the mechanism of the interaction is completely different from that of PIOs, because the involved vibrations typically occur at frequencies above those of the human operator's bandwidth — between 2 Hz and 8 Hz according to Ref. 3 — thus the injected commands are not produced by the pilot's will.

PIO and PAO phenomena have been widely investigated with regard to fixed-wing aircraft (Refs. 4–7). In recent years, rotary-wing aircraft RPC received considerable attention (Refs. 2, 3, 8–10). Ref. 2 reports in the appendix a detailed list of RPC events, which shows a higher incidence of PAO events for rotorcraft than for fixed-wing aircraft. A description of PAO instabilities experienced by US Navy rotorcraft is reported by Walden in Ref. 11.

PAO occurrences about the longitudinal and lateral axes should be less critical in rotorcraft, since changes in cyclic pitch do not cause immediate force imbalance on the vehicle, but rather pitch/roll moments on the rotor, which are usually filtered by the low-pass behavior of common main rotor hub designs, especially articulated ones. However, Walden (Ref. 11) reports that the lateral axis tends to be critical also for PAO, especially when Stability Augmentation Systems (SAS) or more general Automatic Flight Control Systems (AFCS) are present in the Pilot-Vehicle System (PVS). The interaction between the pilot biodynamics and the vehicle dynamics is often amplified by the SAS/AFCS, especially in relation with the roll/lateral axis. However, rotary wing aircraft require artificial stability since they are less stable than conventional fixed wing ones (Ref. 12).

This paper investigates the basic mechanism of aeroservoelastic PAO about the roll axis due to the interaction with the pilot's right arm biomechanics. A simple "closed-loop" numerical model able to represent the basic mechanism of pilot-vehicle interaction is created by connecting a pilot and a vehicle model. The pilot model describes the pilot's biodynamics between the lateral acceleration of the pilot

seat and the lateral stick position. The vehicle model is a 6-degrees of freedom (DOF) analytical model of a helicopter. It includes the cyclic flap and lead-lag main rotor dynamics coupled with the pitch/roll body motions. The connection between the pilot's output and the helicopter's input is realized in the form of a basic AFCS model, which is modeled as a gain-time delay block. A sketch of the proposed model is shown in Fig. 1. The analyzed PAO instability is triggered by the lead-lag regressive main rotor dynamics coupled with the pilot biodynamics, for specific values of gain and time delay on the control line introduced by the AFCS block. It will be shown that the pilot biodynamics reduces the phase margin of the loop transfer function (LTF) of the controlled system when the regressive lead-lag mode is not adequately damped.

This work will show that the basic mechanism of this instability is quite similar to the well known air resonance, in which the airframe roll mode is coupled with the regressive cyclic flap and lead-lag rotor modes (Ref. 13). In the air resonance case, this interaction could lead to a reduction of the damping of the lead-lag mode that brings it at the verge of stability (Ref. 14). This behavior can be sometimes exacerbated by the presence of the SAS/AFCS. The role played by the SAS in the air resonance is taken by the pilot's biodynamics in the Roll/Lateral RPC.

Flight-Simulator Verification of Roll/Lateral RPC

The repeatable occurrence of unstable pilot-assisted oscillation events has been observed on the HE-LIFLIGHT I simulator of the University of Liverpool (UoL), during a test campaign performed in July 2012 within the project ARISTOTEL. A detailed description of the prediction and simulator verification of roll/lateral aeroservoelastic RPCs is described in Ref. 15.

Preliminary experiments were performed to assess the pilot biodynamic feedthrough in relation with the control inputs due to helicopter vibrations. These experiments are reported in detail in Ref. 15.

The pilot/lateral stick dynamics was identified using rational polynomial transfer functions with a third-order denominator and a first-order numerator. Such choice represents a trade-off between complexity and the capability to capture the essence of the experimental frequency response functions. The transfer

function of the structural model equivalent to the pilot/lateral stick dynamics is

$$\frac{\delta_Y}{a_Y^{\text{seat}}} = H_{PP}(s) = -\mu_P \frac{sT_z + 1}{sT_p + 1} \frac{1}{(s/\omega_n)^2 + 2\xi(s/\omega_n) + 1},$$

(1)

where a_Y^{seat} is the acceleration measured in "g" (1 g = 9.81 m/s^2) and δ_Y is the rotation of the cyclic command stick measured in percentage with a range of $\pm 100\%$. The two complex conjugate poles represent the dynamics associated with the pilot biomechanics and the control device. The low frequency real pole represents the integral contribution of the pilot's voluntary action. The zero — usually at high frequency — restores the correct asymptotic behavior of the transfer function. The model of Eq. (1) is consistent with models proposed in the open literature, Refs. 16–18; the pilot transfer functions are similar to the ones measured in-flight and reported in Fig. 6 of Ref. 19.

The identified properties of the three test pilots involved in the campaign are reported in Table 1. The complex conjugate biodynamic poles are well damped, with $\xi > 20\%$ for all pilots. The natural frequencies, ω_n, range between 2 Hz and 3 Hz. It is worth noticing that the static gain μ_P of the transfer function of pilot #1 is significantly higher than that of the other pilots. The differences in the results obtained for pilot #1 are probably related to his anthropometric characteristics: pilot #1 belongs to the 99th percentile for both height and weight, showing somewhat different biomechanical properties from those of an average individual.

One may legitimately ask whether it is possible to decouple the pilot's biodynamics from the dynamics of the control inceptor. It is, indeed, but it requires the capability to separately and independently identify the feedthrough and the admittance of both the pilot and the control inceptor. Whereas it is reasonable to expect some repeatability in the measurement of feedthrough and admittance of the control inceptor, those of the pilot need to be measured simultaneously, posing a non-trivial problem. Several authors have worked on this subject; see for example the theoretical and experimental work of Venrooij et al. (Refs. 20–22) and the numerical models of the pilot's biomechanics and control device dynamics discussed in Refs. 23, 24.

During the testing, PAO occurrences were observed with test pilot #1 while flying the roll step (RS) maneuver. The RS, developed at the UoL for tiltrotor handling qualities evaluation, and subsequently adapted to helicopters (Ref. 25), is a modification of the slalom maneuver defined in Aircraft Design Standards

(ADS) 33, Ref. 26. It is designed to check both the vehicle's ability to maneuver in forward flight and the coordination required to perform the task. The RS maneuver, performed with the aeroservoelastic BO105 at 80 kt, a control gearing ratio of 2.5 times the nominal one and a control time delay τ_Y=100 ms, showed a PAO instability resulting from the coupling of the lightly damped main rotor regressive lead-lag mode at 2.28 Hz with the pilot's lateral dynamics.

An increase in time delay alone beyond 100 ms has been reported in Ref. 27 to reduce the handling qualities of the BO105 from level 1 to level 2. Thus it represents a candidate for the trigger of PIO and PAO when acting together with an increase in the gain G_Y.

Analytical Model for Roll/Lateral Rotorcraft-Pilot Couplings

Numerical predictions of roll/lateral PAO instabilities performed on helicopters with hingeless/bearingless main rotor show that the proximity of the pilot's biodynamic poles to the main rotor lightly damped first regressive lead-lag mode may lead to a reduction of the phase margin of the PVS (Ref. 15). The phenomenon involves the modal participation of the cyclic flap and lead-lag modes and the fuselage roll and pitch dynamics, as for the air resonance, although in the present case interaction occurs with the pilot's biodynamics. The RPC phenomena about the roll axis experienced in the piloted flight simulations presented several similarities with air resonance, a phenomenon that is typical of helicopters with hingeless or bearingless rotors. Compared with articulated main rotors, such rotor designs are capable of building up large hub moments, which enhance the maneuverability and the aircraft response to pilot inputs. Generally, those vehicles are not prone to ground resonance; thus, they seldom have lead-lag dampers, as the aerodynamic in-plane damping is sufficient to stabilize the lead-lag motion. However, in some cases, the lightly damped first lead-lag regressive mode can interact with the flight mechanics modes (body roll and/or pitch), making the system unstable in air (Ref. 14).

The mechanism through which the lateral PAO instability evolves is sketched in Fig. 2. The cycle starts when a voluntary lateral cyclic pitch control is introduced by the pilot into the control chain. Both cosine and sine cyclic coordinates must be taken into account when using multiblade coordinates, since cyclic terms are strongly coupled. The cyclic pitch dynamics modify the angle of attack of each blade,

inducing a flapping motion which in turn tilts the tip path plane of the main rotor, generating pitch and roll moments. The aerodynamic forces produce the main connection between the pitch and the flap dynamics. The Coriolis terms cause a coupling between the flap and the lead-lag motions. A secondary — but non-negligible — contribution originates from the aerodynamic coupling of the lead-lag with the flapping motions. In turn, the cyclic lead-lag modes ζ_{1C} and ζ_{1S} cause an in-plane shift of the rotor center of mass from the axis of rotation, producing roll and pitch moments, and lateral and longitudinal vibrations that are transmitted from the rotor hub to the pilot seat.

The starting point to build an analytical model for roll/lateral RPC are the models originally developed to investigate air resonance, like the one presented in Ref. 28. These models consider 6 degrees of freedom: the two cyclic flap (β_{1C}, β_{1S}), the two cyclic lead-lag (ζ_{1C}, ζ_{1S}), and the two airframe roll and pitch (α_X, α_Y) ones, which are included in the state vector $\mathbf{q}$. The lateral and longitudinal displacements are assumed to have only a minor effect (Ref. 14) and are thus neglected. The aeromechanical system in second-order form is

$$\mathbf{M}\left(\mathbf{p}\right)\mathbf{q}'' + \mathbf{C}\left(\mathbf{p}\right)\mathbf{q}' + \mathbf{K}\left(\mathbf{p}\right)\mathbf{q} = \mathbf{B}\left(\mathbf{p}\right)\mathbf{u}, \tag{2}$$

$$y = R\Omega^2 \mathbf{D}\mathbf{q}'' \tag{3}$$

where matrices $\mathbf{M}$, $\mathbf{C}$ and $\mathbf{K}$ include both the structural and aerodynamic contributions, which are functions of the trim parameters $\mathbf{p}$. The superscript $(\cdot)'$ denotes the derivative with respect to the azimuthal coordinate $\psi = \Omega \cdot t$. The control vector $\mathbf{u}$ contains the lateral and longitudinal cyclic pitch angles, namely $\mathbf{u} = \{\vartheta_{1C}; \vartheta_{1S}\}$. The output y represents the lateral acceleration measured at the pilot's seat, e.g. $y = a_Y^{seat}$, which can be expressed as a linear combination of the second derivative of the coordinate vector elements, $\mathbf{q}''$. The elements of the matrices can be found in the referenced papers.

The relationship between the two inputs and the output is

$$y(s) = s^2 R\Omega^2 \mathbf{D}\left(\mathbf{M}\left(\mathbf{p}\right)s^2 + \mathbf{C}\left(\mathbf{p}\right)s + \mathbf{K}\left(\mathbf{p}\right)\right)^{-1}\mathbf{B}\left(\mathbf{p}\right)\mathbf{u}(s). \tag{4}$$

It is characterized by two transfer functions

$$a_Y^{seat} = H_{YC}(s,\mathbf{p})\,\vartheta_{1C} + H_{YS}(s,\mathbf{p})\,\vartheta_{1S}. \tag{5}$$

The lightly damped low frequency vibrations due to the lead-lag regressive mode can interact with the

pilot's biomechanics along the sway axis, which are in the range of 2–3 Hz, and thus feed back in the form of involuntary lateral controls to the main rotor dynamics. Usually, the lateral PAO instability arises when an AFCS is included in the PVS. Specifically, the introduction of a gain and a time delay between the pilot's demand and the servoactuators displacement may reduce the PVS gain and phase margins.

Validation of the model

The proposed 6-DOF Air Resonance (AR) model is compared with the BO105 aeroelastic model used in the piloted flight simulator campaign to check whether the analytical model adequately represents the tat areessential dynamicsbasic elements required to predict the instability. This helicopter was selected because it is representative of light-weight, hingeless helicopters and the required data is publicly available. A detailed validation of the model used for the flight simulator using flight test results from the open literature is presented in Ref. 15.

The full-state aeroservoelastic BO105 has been realized in MASST (Modern Aeroservoelastic State Space Tools), a tool for the aeroservoelastic and aeromechanical analysis of aircraft and rotorcraft (Refs. 29, 30). MASST models vehicles as Linear Time Invariant (LTI) systems, computed using coefficient averaging to eliminate any periodicity whenever the rotors are not in axial flow conditions. The airframe has been modeled as a rigid body. The rotor has been modeled considering 3 bending modes, 2 torsion modes, and the 3 state Pitt-Peters dynamic inflow model (Ref. 31). A rigid teetering model is used for the tail rotor, considering the coning and teetering modes. Linear servoactuator transfer functions are defined for the three actuators of the main rotor swashplate and for the single actuator of the tail rotor. The model includes sensors for positions, velocities and accelerations at the pilot seat in the longitudinal, lateral and vertical directions, and three sensors for measuring the roll, pitch and yaw angular rates p, q, r. Finally, the airframe stability derivatives, resulting from the contribution of the fuselage/wing body (WB), the horizontal tail (HT), and the vertical tail (VT) have been estimated using the aerodynamic coefficients look-up tables provided in Ref. 12, to take into account the low-frequency flight dynamics behavior. The general characteristics of the aircraft where taken from Refs. 3, 12.

The full-state MASST model consists of 62 states. The corresponding roots are characterized by

hybridized mode shapes. The root locus of the BO105 in hover, Sea Level Standard (SLS) ISA + 0° conditions is shown in Fig. 3(a) up to 110 rad/s. The full-state MASST model is able to represent the low frequency eigenvalues associated with the relevant flight mechanics modes (see Fig. 3(b), bottom). Dutch roll, phugoid, heave subsidence and spiral modes show the trends reported in Chapter 4 of Ref. 12. Long-period pitching oscillations, related to the phugoid dynamics, are unstable. The effect of the dynamic inflow model is significant on the flap/rigid body modes, which are associated with the longitudinal and lateral dynamics of the rotor tip path plane coupled with the body angular rates. Flap roots are well damped, whereas the lead-lag regressive and progressive poles are located quite close to the imaginary axis, as shown in Fig. 3. As expected, the regressive lead-lag natural frequency is small compared with helicopters of the same class featuring an articulated main rotor.

The eigenvalues of the full-state MASST model are compared with those obtained with the 6-DOF Air Resonance model. Table 2 lists the eigenvalues and the corresponding mode shapes of the 6-DOF Air Resonance model in the same hover conditions. The eigenanalysis returns two real and four complex conjugate poles. The open loop system is stable since all roots have negative real parts. Pitch and roll subsidence roots, related to the helicopter stability derivatives $M_{/q}$ and $L_{/p}$, are well captured (see Ref. 12).

Several differences can be noticed. The full-state MASST flap progressive mode is quite close to the corresponding mode obtained with the 6-DOF Air Resonance model, although less damped. The difference is caused by the absence of inflow dynamics in the Air Resonance model. The lead-lag regressive and progressive frequencies correlate well, but the MASST lead-lag roots are less damped. In particular, the damping predicted by the Air Resonance model is more than twice that predicted using MASST (4.27% vs. 2.01%, Fig. 3(b)). Finally, the low frequency flap regressive mode computed by MASST is coupled with the pitch and the roll subsidence modes, generating two complex conjugate roots. This is related to the interaction between the pitch and roll airframe dynamics and the inflow lateral and longitudinal dynamics, which reduce the aerodynamic loads during the transients and the modal damping of the flap dynamics.

A further comparison of the two dynamical models has been performed in terms of transfer function (TF) between the lateral cyclic pitch ϑ_{1C} and the lateral acceleration at the pilot's seat a_Y^{seat}. This is the

Loop Transfer Function that is used in Nyquist's criterion to analyze the stability and the robustness of the PVS. The Bode plot of $H_{YC}(s, \mathbf{p})$, in Hover SLS, is shown in Figure 4.

The static gain and the initial slope of the two TFs are clearly different since the MASST model contains the low frequency dynamics related to flight mechanics, whereas the phase angles show a similar trend between 0.1 Hz and 1 Hz. The slightly higher phase angle of the MASST model is mainly related to inflow dynamics as reported by Kaplita et al. in Ref. 32. The lead-lag regressive peak is clearly visible at about 2 Hz on both models. However, the Air Resonance model shows a higher damping since the magnitude of the peak is lower. The effects of the rigid fuselage lateral mode and of the servoactuator second-order dynamics (with a cut-off frequency of about 10 Hz) reduce the phase angle on the MASST TF in the bandwidth between 2.5 Hz and 10 Hz. At frequencies above 10 Hz, the peak of the lead-lag progressive mode can be noticed, respectively at 12.3 Hz for the 6-DOF AR model and 12.7 Hz for the full state MASST model.

Figure 5(b) shows the transfer function between the lateral cyclic input and the lateral acceleration at the pilot seat with and without dynamic inflow as predicted by the detailed MASST model. The addition of the dynamic inflow decreases the response amplitude and slightly increases the phase in the frequency region up to 1 Hz. However, the lead-lag dynamics is not modified and no differences can be noticed in the 2–8 Hz band interested by the aeroelastic-pilot biomechanics phenomena. As a consequence, the dynamic inflow, which significantly affects the roots position, can be initially neglected for lateral PAO analysis. In conclusion, the analytical model represents quite reasonably the essential dynamics in the bandwidth of interest. However, there are important shortcomings of the analytical model. In particular, the 6-DOF Air Resonance model overestimates the damping of the lead-lag regressive mode. This is not conservative for PAO predictions along the lateral axis, since the regressive lead-lag damping can have a critical impact on the robust stability margins of the PVS (Ref. 15).

The correct regressive lead-lag modal damping can be retrieved by including the statically residualized effect of the cyclic pitch dynamics on the air resonance equations. Pitch dynamics are usually characterized by higher frequencies when compared with the first flap or lead-lag dynamics ans thus can be neglected. However, static torsional compliance causes a non-negligible effect on the low frequency dynamics, which is essential to recover the correct lead-lag peak damping of the pitch-lateral acceleration

TF. The importance of the static torsional compliance has been highlighted also for other RPC phenomena in Refs. 33, 34.

The eigenvalues obtained with the updated model are reported in Table 3. The main effect is observed on the lead-lag regressive damping that decreases from 4.27% of the original 6-DOF Air Resonance model to 2.19% for the 6-DOF Air Resonance model with residualized pitch dynamics, a value much closer to that of the full state MASST model, i.e. 2.01%. Although the obtained modal damping is slightly greater than the corresponding value obtained in MASST, the 6-DOF Air Resonance model can now be considered adequate for preliminary studies of roll/lateral PAO phenomena. The eigenvalues are compared with those obtained using MASST in Fig. 6.

The effect of the lightly damped lead-lag regressive mode can be observed also in the Bode plot of the TF between ϑ_{1C}^{con} and a_Y^{seat}, which is shown in Fig. 7.

Pilot-in-the-loop stability

Using the analytical model developed in the previous sections, the stability of the coupled rotorcraft-pilot loop and its sensitivity to several design parameters can be investigated. Instead of using the classical eigenanalysis, the robust stability analysis approach can be exploited, because it gives qualitative and quantitative information about stability with respect to parameter variations (Refs. 35, 36). Hence, stability analysis is performed using complex-variable transfer functions and exploiting the Nyquist criterion (Ref. 37). In this case, the criterion can be formulated as: given a single input single output (SISO) dynamic system $H(s)$ and an uncertainty operator $K(s) = G_Y e^{-s\tau_Y}$, where G_Y is a positive real number greater than 1 and τ_Y is a positive number representing a time delay, that are in feedback loop, the system is marginally stable whenever the frequency response of the Loop Transfer Function (LTF) $P(\mathrm{j}\omega) = H(\mathrm{j}\omega)K(\mathrm{j}\omega)$ crosses the critical point in the complex plane $(-1 + \mathrm{j}0)$ (see Ref. 38 for a proof). In this specific case, the nominal LTF can be easily obtained by directly feeding the pilot/lateral stick dynamic model (1) into the vehicle model

$$H_{\mathrm{nom}}(s, \mathbf{p}) = -G_{1C}\, H_{PP}(s)\, H_{YC}(s, \mathbf{p}), \tag{6}$$

where G_{1C} is the gearing ratio between the lateral stick displacement and the rotor lateral cyclic pitch. For the BO105 model used in the flight simulator it was $G_{1C} = -0.05$ deg/%. The minus sign in Eq. (6) is introduced because the pilot contribution provides a negative feedback loop closure.

The uncertainty operator represents a possible variation of gain or time delay that may be introduced in the control loop by the simplified AFCS. Consequently, the stability boundary can be found analytically by solving this complex equation for $\hat{G}_Y(\omega)$ and $\hat{\tau}_Y(\omega)$

$$\hat{G}_Y e^{-\mathrm{j}\omega\hat{\tau}_Y} H_{\mathrm{nom}}(\mathrm{j}\omega, \mathbf{p}) = -1, \tag{7}$$

for all frequencies $\omega \in [-\infty, +\infty]$. This means that

$$\hat{G}_Y = \left| \frac{1}{H_{\mathrm{nom}}(\mathrm{j}\omega, \mathbf{p})} \right| \tag{8}$$

$$\theta(\omega) = \tan\left(\hat{\tau}_Y \omega\right) = -\frac{\Im(H_{\mathrm{nom}}(\mathrm{j}\omega, \mathbf{p}))}{\Re(H_{\mathrm{nom}}(\mathrm{j}\omega, \mathbf{p}))}, \tag{9}$$

so Bode plots of $H_{\mathrm{nom}}(\mathrm{j}\omega)$ can be used to evaluate $\hat{G}_Y(\omega)$ and $\hat{\tau}_Y(\omega)$. For instability to occur, the control loop gain G_Y must increase such that the LTF exceeds 0 dB and the time delay τ_Y must increase to a point that the phase margin is depleted.

The Nyquist plot of the detailed BO105 MASST model connected to the biodynamic model of pilot #1 at a gain of $G_Y \geq 2.5$ and for a time delay of 140 ms (obtained by summing the delay of 100 ms to the flight simulator filters and hardware time delay of about 40 ms), is shown in Fig. 8 for several flight velocities. It is clear that at 80 kt the model predicts a marginally stable system, while the experiments found an incipient instability. Consequently, it can be stated that the numerical model reasonably predicts the stability of the actual system (see Ref. 15). In addition, Fig. 8 shows that increasing the flight speed further reduces the stability margins. However, the proneness is clearly shown also by the hover Nyquist plot; as a consequence, using a model designed for hover to consider the proneness of the vehicle during the initial sizing seems an acceptable approximation.

Sensitivity of Stability to Design Parameters

The availability of an analytical model for the hover case gives the designer the opportunity to perform a sensitivity analysis for the main helicopter design parameters $\mathbf{p}$, to understand what are the characteris-

tics that mainly influence the stability margins.

Figure 9 compares the results obtained for nominal conditions considering the biodynamics of the three identified test pilots in feedback loop with the BO105 in Hover, SLS flight conditions. The differences between the three pilots are clearly visible. The stability map in Fig. 9(a) shows a higher tendency to lateral PAO phenomena of pilot #1 than the other test pilots. This is due to the higher static gain of the pilot's biodynamic TF (see Table 1) of this pilot, that increases the magnitude of the corresponding $H_{nom}(s, \mathbf{p})$ (see Fig. 9(b)). Moreover, the LTF of test pilot #1 is also the one characterized by the largest phase delay.

Figure 9 shows that without the introduction of some time delay, the gain G_Y alone is not sufficient to destabilize the PVS. So it is the phase shift of the LTF rather than than the amplification that may cause a lateral PAO phenomenon. All curves of Fig. 9(a) present a minimum at a particular value of time delay. The lowest uncertainty operator gain necessary to achieve the marginal stability condition occurs at this minimum value. For test pilot #1, this point is reached with a time delay of about 200 ms, for which a small value of G_Y, slightly higher than 1, is sufficient to trigger a roll/lateral PAO.

To understand the dependence of these stability maps from the design parameters of a rotorcraft, $\mathbf{p}$, several sensitivity analyses have been performed, exploiting the knowledge of the analytical dependence of the model on the parameters. These analyses have been performed considering only pilot #1, since it was the most prone to the lateral RPC.

Sensitivity to rotorcraft inertia

The effect on the lateral PAO stability of varying rotorcraft roll and pitch inertia from their baseline values is shown in Fig. 10.

Both roll and pitch inertia have been modified by $\pm 10\%$. The stability maps clearly show that changes in roll inertia I_{xx} produce more remarkable effects than those in the pitch inertia I_{yy}. This is essentially related to the kinematic connection of the lateral pilot's seat acceleration with the CM roll acceleration. Cross-coupling effects between the helicopter roll and pitch dynamics are always present (due to the cross-terms of the inertia tensor, gyroscopic and aerodynamics terms). This explains the small variation of the

stability maps when the pitch inertia is also modified, although it appears negligible when compared to that of the roll inertia.

Figure 10(a) shows that a relatively small reduction in body roll inertia decreases the gain G_Y on the stability boundaries. For given values of stability and control derivatives associated with the rotor, the lateral acceleration of the vehicle, which is fed to the involuntary pilot model, is scaled by a factor inversely proportional to the helicopter roll inertia.

In both cases, the modification of the rotorcraft inertia causes a reduction of the stability margins when I_{xx} or I_{yy} decrease and an increment of stability margins when either values increase. The reduction of the margin is more sensible for the gain $\hat{G}_Y$ than for the time delay $\hat{\tau}_Y$.

It should be noted that when the roll and pitch inertia are reduced, the stability maps show unstable conditions also for values of the control loop gain G_Y lower than 1. In general, for all these cases the robust analysis indicates that time delay alone suffices to trigger the PAO condition; considering that for nominal, i.e. unitary, control loop gain the stability boundaries have been already crossed. Clearly, a reduction of the control loop gain may restore stability (at the very least, for $G_Y = 0$, i.e. when the pilot leaves the control inceptor, the feedback loop is interrupted).

Sensitivity to Lock number

Figure 11 shows the stability map and the LTF for different values of Lock number ($\gamma_{nom}\pm10\%$). The Lock number, a parameter that expresses the ratio between the aerodynamic and inertia flap moments, $\gamma = \rho a c R^4/I_\beta$, has been modified for constant inertia properties, thus virtually changing the aerodynamic properties.

Figure 11(a) clearly shows that reducing the Lock number adversely affects the stability of the PVS resulting from involuntary pilot control closure on the lateral cyclic control inceptor. The Lock number is directly proportional to the aerodynamic forces, developing the only source of aerodynamic damping on the lead-lag roots. When the Lock number reduces, the lead-lag regressive peak on the Bode plot of Fig. 11(b) becomes more pronounced and the phase margin reduces as well. The negative effect on both the magnitude and the phase of the LTF leads to an increment of the unstable area in the G_Y, τ_Y plane.

Since the Lock number is proportional to the air density, ρ, it changes with the operating conditions. For example, when operating at ISA -40°C, the air density increases of about 15%; when operating at 15000 ft the air density decreases of about 35%. As a consequence, a variability even higher than that shown in Fig. 11 can be observed within operational conditions.

Sensitivity to rotor speed

Figure 12 refers to modifications of the rotor speed. The variation, realized keeping constant the non-dimensional flap, lead-lag and pitch frequencies, varies the frequencies of the rotating system with respect to those of the pilot, which is constant in the non-rotating system. The frequency of the lead-lag regressive root increases from 2.22 Hz to 2.45 Hz for $\Omega_{\text{nom}} + 10\%$ and decreases to 2.00 Hz for $\Omega_{\text{nom}} - 10\%$.

The variation of Ω by $\pm 10\%$ moves in both cases the dimensional lead-lag regressive frequency away from the biomechanical frequency of the test pilot. Consequently, a general light reduction of the LTF magnitude is observed, which in turn causes a slight increase of $\hat{G}_Y$. However, when Ω is increased, the phase margin further reduces at the pilot-lag regressive frequency, and the lateral PAO stability limit is reached for lower values of τ_Y.

Sensitivity to rotor frequencies

Sensitivity to rotor frequencies is analyzed separately, since the effects of the flap, lead-lag and blade pitch dynamics on the lateral PAO phenomenon are different. Figure 13 shows the stability map and the Bode plot of the nominal LTF for small perturbations of the non-dimensional flap frequency $\nu_{\beta_{\text{nom}}} \pm 3\%$.

A more reactive rotor ($\nu_\beta + 3\%$) increases the magnitude of the nominal LTF, reducing the phase delay in proximity of the lead-lag regressive root. The combined effect leads to a drastic reduction of $\hat{G}_Y$, but also to an increase of the time delay necessary for instability. Reducing the flap frequency, the effect is opposite, since the stability boundaries are characterized by higher gains G_Y and lower time delays. The reduction of ν_β leads to a rapid increase of the gain required to drive the system unstable, which reaches values unrealistic for a helicopter. This explains why this type of RPC is not expected with articulated rotors, as proved experimentally with the flight simulator tests performed using an aeroservoelastic model

of the IAR330 PUMA (Ref. 15).

Sensitivity to lead-lag frequency has been investigated for 3 perturbation values, namely $\nu_{\zeta_{\text{nom}}} \pm 5\%$ and $\nu_\zeta = 1.5 \cdot \nu_{\zeta_{\text{nom}}} = 1.005$/rev. The last value has been considered to address the case of a stiff-inplane rotor. Figure 14 shows the stability map and the Bode plot of the nominal LTF for the different values of the lead-lag frequency. For $\nu_{\zeta_{\text{nom}}} + 5\%$ the regressive lead-lag root decreases to 2.01 Hz and the corresponding peak on the magnitude Bode plot of Fig. 14(b) slightly increases, reducing the gain G_Y required to make the system unstable. However, there is a reduction of the phase angles, so higher time delays are necessary to reach a lateral PAO condition as shown in Fig. 14(a). Conversely, for $\nu_{\zeta_{\text{nom}}} - 5\%$ the dimensional frequency increases up to 2.44 Hz, the PVS gain margin G_Y increases but the phase delay is reduced.

For lead-lag frequencies above 1/rev, the lead-lag regressive peak and phase delay disappear from the nominal LTF shown in Fig. 14(b). Lateral PAO instabilities are reached for higher gains and unrealistic time delays, as depicted by the dashed line of Fig. 14(a). The regressive lead-lag dynamics does not amplify the phenomenon any more, although it remains present.

The importance of the static residualization of the blade pitch cyclic equations on the lead-lag dynamics has been discussed in previous sections. So the blade pitch non-dimensional frequency, which is related to the torsional compliance of the blades, may have an effect on the RPC. Stability maps obtained by perturbing the blade pitch frequency are shown in Fig. 15(a). A strong reduction of the blade pitch frequency, due for example to a more compliant control chain, decreases the damping of the lead-lag regressive root and thus increments the magnitude of the LTF and reduces the phase (see Fig. 15(b)). The effect on the stability map is destabilizing since it reduces the gain G_Y and the time delay required to become unstable when $\nu_\vartheta = 80\% \nu_{\vartheta_{\text{nom}}}$. On the contrary, the lateral PAO stability boundaries improve when the pitch frequency increases.

Sensitivity to rotor trim angles

The increment of specific rotor thrust, i.e. C_T/σ, leads essentially to an increment of the rotor coning angle β_0 and of the collective pitch angle ϑ_0. So, it is worth checking the dependence of the stability from

these trim geometric parameters. Stability maps have been evaluated for perturbations of ± 0.5 deg from the nominal trim conditions.

Increasing the rotor coning angle β_0 increases the in-plane Coriolis moments due to the relative flapping motion. This reduces the regressive lead-lag mode damping and negatively impacts on the magnitude and phase delay of the LTF, significantly decreasing the stability margins, as shown in Fig. 16(a).

On the other side, the collective pitch trim angle ϑ_0 acts only on the generalized aerodynamic forces, increasing the damping of the regressive lead-lag mode when $\Delta\vartheta_0 > 0$ and thus moving the stability boundaries at higher gains and time delays, as depicted in Fig. 16(b).

The trend of the trim parameters with respect to the specific rotor thrust for the specific helicopter under analysis is reported in Fig. 17(a). The nominal condition is characterized by $C_T/\sigma = 0.065$. The sensitivity analysis of Fig. 17(b) has been performed for small perturbations of $C_T/\sigma \pm 0.005$, corresponding to a thrust variation of about ± 1500 N. The 6-DOF analytical model has been updated consistently, considering the trim values of Fig. 17(a). Although the increment of collective pitch is greater than the rotor coning angle, for specific rotor thrust variations the effect of in-plane Coriolis moments dominates on the generalized aerodynamic forces, reducing the lead-lag damping and thus decreasing the roll/lateral PAO stability boundaries.

Effect of lead-lag viscous damping

Introducing a lead-lag viscous damping C_b on the blades increases the stability margins with respect to lateral PAO. In fact, increasing the damping of the lead-lag regressive mode reduces the magnitude and the phase delay of the LTF.

Figure 18 shows the effect of C_b on the stability maps. Two values of non-dimensional damping $C_b/I_b\Omega$, $1.35 \, 10^{-2}$ and $2.70 \, 10^{-2}$, have been considered. They increase the lead-lag regressive damping from 2.19% to 4.59% and 6.98%, respectively. The results show that when the lead-lag regressive mode damping increases, the stability boundaries move towards higher gains and time delays.

Effect of pitch-flap and pitch-lag kinematic couplings

Figure 19 shows the changes in the stability boundaries when the blade kinematic coupling parameters K_{p_β} and K_{p_ζ} are modified.

A negative kinematic pitch-flap coupling, K_{p_β}, significantly reduces the stability to lateral PAO phenomena, especially in terms of gain (see Fig. 19(a)). Conversely, a positive pitch-flap coupling, obtained with a δ_3 angle of about 26 degrees, significantly improves stability, moving the boundaries toward very high gains and time delays.

Negative kinematic pitch-lag coupling, K_{p_ζ}, (i.e. the blade pitches down as it leads) has a stabilizing effect on PAO proneness, as shown in Fig. 19(b). This coupling has little influence on the frequencies; nevertheless, the lead-lag regressive damping is improved. This is consistent with the results described in Ref. 14 for the air resonance case.

Effect of longitudinal cyclic stick biodynamic feedthrough

The last sensitivity analysis addresses the cross-coupling of a longitudinal cyclic stick input combined with the nominal lateral one. In fact, although a single lateral acceleration is introduced in the cockpit, the pilot's right hand generally moves in a direction that is a combination of the lateral and longitudinal directions. A simple cross-coupling effect can be modeled considering a longitudinal cyclic stick displacement proportional to the lateral one, i.e. $\delta_X = C_{XY} \, \delta_Y$, through a cross-coupling factor C_{XY}. The nominal LTF used by the Nyquist criterion becomes

$$H_{\text{nom}}(s, \mathbf{p}) = -G_{1C} \, H_{PP}(s) \left[H_{YC}(s, \mathbf{p}) + C_{XY} \, \frac{G_{1S}}{G_{1C}} \, H_{YS}(s, \mathbf{p}) \right],$$ (10)

where G_{1S} is the gearing ratio between the longitudinal stick displacement and the rotor longitudinal cyclic pitch. For the BO105 model used in the UoL flight simulator, the coefficients were estimated as $G_{1C} = G_{1S} = 0.09$ deg/%. The effect of the cross-coupling on the stability maps and on the LTF is shown in Fig. 20. Stability maps have been evaluated for cross-coupling factors of $C_{XY} \pm 30\%$. For $C_{XY} > 0$ a right (left) stick displacement involves a longitudinal stick pull (push). The main effect on the nominal LTF is the modification of the zero associated with the lead-lag regressive pole. A negative cross-coupling

reduces the control loop gain $\hat{G}_Y$. The opposite behavior occurs when C_{XY} is positive, although the time delay is lightly reduces.

Conclusions

This paper presents a simple closed-loop numerical model that is able to predict the basic mechanism of roll/lateral PAO phenomena occurring on rotors in hover conditions. The proposed model is based on the 6-DOF differential equations developed for air resonance analysis, which have been coupled with a biomechanical model of the pilot.

When air resonance occurs, the airframe roll mode couples with the regressive cyclic flap and lead-lag rotor modes, driving the lightly damped regressive lead-lag mode unstable. In the case of roll/lateral RPC, the regressive lead-lag mode becomes unstable due to its proximity with the pilot's biomechanical roots. This work showed that this type of instability may arise when a AFCS included in the lateral cyclic control loop introduces a phase shift through a time delay. Without the required amount of time delay this instability is unlikely to develop, unless very high gearing ratios are used in the cyclic pitch control chain.

The simple analytical model presented in this work made it possible to investigate the sensitivity of this kind of phenomenon with respect to several important design parameters of rotorcraft.

It wasshown that articulated rotors are not expected to suffer from this problem, whereas hingeless and bearingless soft-inplane rotors may be prone to this type of RPC. Additionally, by increasing the rotor loading there is a reduction of both the time delay and the control loop gain required to destabilize the pilot-vehicle system.

There appears to be a noteworthy similarity between air resonance (caused by FCS) and PAO instability caused by interaction between the helicopter and the pilot. The pilot's involuntary biodynamic feedthrough introduces some amplification and phase delay in a narrow frequency band that is close to that of the main rotor's regressive lead lag. This may reduce the stability margins of the closed-loop pilot-vehicle system. As a consequence, a phenomenon similar to air resonance may occur also in rotorcraft without a sophisticated FCS or, when a FCS is present, the pilot's involuntary biodynamics may further reduce stability margins.

The availability of a simple analytical model as the one presented here may provide designers with useful indications of the sensitivity of helicopters to this kind of problem leading to actions — often in terms of lead-lag damping increment — that may avoid more substantial redesign actions at later stages. The previously mentioned sensitivities, estimated using the analytical model, have not been verified by dedicated test campaigns. However, the piloted flight simulations this numerical study builds upon, and the associated sensitivity of the baseline BO105 helicopter to gain and time delay, were correctly reproduced by the numerical models. As a consequence, it is inferred that the sensitivity analysis is based on solid foundations.

Changes to inceptor configuration or dynamics, e.g. modifications of its position in the cockpit or of its damping, stiffness or inertia, were not considered as means of mitigation. Such changes may be quite effective in reducing the proneness of the pilot-vehicle system to this type of RPCs. However, the current numerical capabilities to identify and model the pilot-inceptor dynamics do not allow to estimate the effect of those changes. Changing the inceptor type and position will change the configuration of the pilot's limbs and consequently its feedthrough and admittance. Changing the inceptor characteristics will change the muscular tension in the pilot's arm and thus its admittance. More sophisticated biomechanical models, validated through dedicated test campaigns, would be required to achieve the capability to predict the effect of those changes by means of numerical models rather than directly by means of in-flight test.

Acknowledgments

References

[1]McRuer, D. T., *Aviation Safety and Pilot Control: Understanding and Preventing Unfavourable Pilot-Vehicle Interactions*, Washington DC: National Research Council, National Academy Press, 1997.

[2]Pavel, M. D., Jump, M., Dang-Vu, B., Masarati, P., Gennaretti, M., Ionita, A., Zaichik, L.,

Smaili, H., Quaranta, G., Yilmaz, D., Jones, M., Serafini, J., and Malecki, J., "Adverse rotorcraft pilot couplings — Past, present and future challenges," *Progress in Aerospace Sciences*, Vol. 62, doi:10.1016/j.paerosci.2013.04.003, October 2013, pp. 1–51.

[3]Dieterich, O., Götz, J., DangVu, B., Haverdings, H., Masarati, P., Pavel, M. D., Jump, M., and Gennaretti, M., "Adverse Rotorcraft-Pilot Coupling: Recent Research Activities in Europe," Proceeding of the 34th European Rotorcraft Forum, September 16–19 2008.

[4]AGARD, "PIO Workshop following Active Control Technology: Applications and Lessons Learned," CP 560, AGARD, 1995.

[5]Klyde, D. H. and Mitchell, D. G., "A PIO Case Study — Lessons Learned Through Analysis," Proceeding of the AIAA Atmospheric Flight Mechanics Conference, August 15–18 2005.

[6]Perng, J.-W., "Application of parameter plane method to pilot-induced oscillations," *Aerospace Science and Technology*, Vol. 23, (1), doi:10.1016/j.ast.2011.06.006, December 2012, pp. 140–145.

[7]Weltz, G., Shweyk, K., and Murray, D., "Application of New and Standard Pilot-Induced Oscillation (PIO) Analysis Methods to Flight Test Data of the C-17 Transport Aircraft," Proceeding of the AIAA Atmospheric Flight Mechanics Conference and Exhibit, August 20–23 2007.

[8]Pavel, M. D., Malecki, J., DangVu, B., Masarati, P., Gennaretti, M., Jump, M., Smaili, H., Ionita, A., and Zaicek, L., "A Retrospective Survey of Adverse Rotorcraft Pilot Couplings in European Perspective," Proceeding of the 68th Annual Forum of the American Helicopter Society, May 1–3 2012.

[9]Pavel, M. D., Masarati, P., Gennaretti, M., Jump, M., Zaichik, L., Dang-Vu, B., Lu, L., Yilmaz, D., Quaranta, G., Ionita, A., and Serafini, J., "Practices to identify and preclude adverse Aircraft-and-Rotorcraft-Pilot Couplings — A design perspective," *Progress in Aerospace Sciences*, Vol. 76, doi:10.1016/j.paerosci.2015.05.002, 2015, pp. 55–89.

[10]Pavel, M. D., Yilmaz, D., Stroosma, O., Dang-Vu, B., Masarati, P., Quaranta, G., Gennaretti, M., Jump, M., Lu, L., Jones, M., Smaili, H., and Zaichik, L., "Practices for Identifying and Precluding Adverse Aircraft- and Rotorcraft-Pilot Couplings Events — Simulator Guidelines," *Progress in Aerospace Sciences*, Vol. 77, doi:10.1016/j.paerosci.2015.05.007, August 2015, pp. 54–87.

[11]Walden, R. B., "A Retrospective Survey of Pilot-Structural Coupling Instabilities in Naval Rotorcraft," Proceeding of the 63rd Annual Forum of the American Helicopter Society, May 1–3 2007.

[12]Padfield, G. D., *Helicopter Flight Dynamics: The Theory and Application of Flying Qualities and Simulation Modelling*, Blackwell Publishing, 2007.

[13]Donham, R. E., Cardinale, S. V., and Sachs, I. B., "Ground and Air Resonance Characteristics of a Soft In-Plane Rigid-Rotor System," *Journal of the American Helicopter Society*, Vol. 14, (4), doi:10.4050/JAHS.14.33, 1969, pp. 33–41.

[14]Milgram, J. H. and Chopra, I., "Air Resonance of Hingeless Rotor Helicopters in Trimmed Forward Flight," *Journal of the American Helicopter Society*, Vol. 39, (4), October 1994, pp. 46–58.

[15]Muscarello, V., Quaranta, G., Masarati, P., Lu, L., Jones, M., and Jump, M., "Prediction and Simulator Verification of Roll/Lateral Adverse Aeroservoelastic Rotorcraft-Pilot Couplings," *J. of Guidance, Control, and Dynamics*, Vol. 39, (1), doi:10.2514/1.G001121, January 2016, pp. 42 – 60.

[16]Allen, R. W., Jex, H. R., and Magdaleno, R. E., "Manual Control Performance and Dynamic Response During Sinusoidal Vibration," TR 73-78, AMRL, October 1973.

[17]Jex, H. R. and Magdaleno, R. E., "Biomechanical models for vibration feedthrough to hands and head for a semisupine pilot," *Aviation, Space, and Environmental Medicine*, Vol. 49, (1–2), 1978, pp. 304–316.

[18]Höhne, G., "Computer aided development of biomechanical pilot models," *Aerospace Science and Technology*, Vol. 4, (1), doi:10.1016/S1270-9638(00)00117-6, January 2000, pp. 57–69.

[19]Parham, T., Jr., Popelka, D., Miller, D. G., and Froebel, A. T., "V-22 Pilot-in-the-loop Aeroelastic Stability Analysis," Proceeding of the 47th Annual Forum of the American Helicopter Society, May 6–8 1991.

[20]Venrooij, J., Mulder, M., Abbink, D. A., van Paassen, M. M., Mulder, M., van der Helm, F. C. T., and Bülthoff, H. H., "A New View on Biodynamic Feedthrough Analysis: Unifying the Effects on Forces and Positions," *IEEE Trans. on Systems, Man, and Cybernetics, Part B: Cybernetics*, Vol. 43, (1), doi:10.1109/TSMCB.2012.2200972, 2013, pp. 129–142.

[21]Venrooij, J., van Paassen, M., Mulder, M., Abbink, D., Mulder, M., van der Helm, F., and Bulthoff, H., "A Framework for Biodynamic Feedthrough Analysis Part I: Theoretical Foundations," *Cybernetics, IEEE Transactions on*, Vol. 44, (9), doi:10.1109/TCYB.2014.2311043, September 2014, pp. 1686–1698.

[22]Venrooij, J., van Paassen, M., Mulder, M., Abbink, D., Mulder, M., van der Helm, F., and Bulthoff, H., "A Framework for Biodynamic Feedthrough Analysis Part II: Validation and Application," *IEEE*

Transactions on Cybernetics, Vol. 44, (9), doi:10.1109/TCYB.2014.2336375, September 2014, pp. 1699–1710.

[23]Masarati, P. and Quaranta, G., "Bioaeroservoelastic Analysis of Involuntary Rotorcraft-Pilot Interaction," *J. of Computational and Nonlinear Dynamics*, Vol. 9, (3), doi:10.1115/1.4025354, July 2014, pp. 031009.

[24]Zanlucchi, S., Masarati, P., and Quaranta, G., "A Pilot-Control Device Model for Helicopter Sensitivity to Collective Bounce," Proceeding of the ASME IDETC/CIE 2014, August 17–20 2014.

[25]Cameron, N. and Padfield, G. D., "Handling Qualities Degradation in Tilt-Rotor Aircraft Following Flight Control System Failures," Proceeding of the 30th European Rotorcraft Forum, September 14-16 2004.

[26]Anonymous, "Performance Specification, Handling Qualities Requirements for Military Rotorcraft," ADS 33-E-PRF, US Army AMCOM, Redstone, Alabama, 2000.

[27]Pausder, H. J. and Blanken, C. L., "Investigation of the Effects of Bandwidth and Time Delay on Helicopter Roll-Axis Handling Qualities," Proceeding of the 18th European Rotorcraft Forum, September 15–18 1992.

[28]Gandhi, F. and Chopra, I., "An Analytical Model for a Nonlinear Elastomeric Lag Damper and Its Effect on Aeromechanical Stability in Hover," *Journal of the American Helicopter Society*, Vol. 39, (4), October 1994, pp. 59–69.

[29]Masarati, P., Muscarello, V., and Quaranta, G., "Linearized Aeroservoelastic Analysis of Rotary-Wing Aircraft," Proceeding of the 36th European Rotorcraft Forum, September 7–9 2010.

[30]Masarati, P., Muscarello, V., Quaranta, G., Locatelli, A., Mangone, D., Riviello, L., and Viganò, L., "An Integrated Environment for Helicopter Aeroservoelastic Analysis: the Ground Resonance Case," Proceeding of the 37th European Rotorcraft Forum, September 13–15 2011.

[31]Pitt, D. M. and Peters, D. A., "Theoretical Prediction of Dynamic-Inflow Derivatives," *Vertica*, Vol. 5, (1), 1981, pp. 21–34.

[32]Kaplita, T. T., Driscoll, J. T., Diftler, M. A., and Hong, S. W., "Helicopter simulation development by correlation with frequency sweep flight test data," Proceeding of the 45th Annual Forum of the American Helicopter Society, May 22–24 1989.

[33]Serafini, J., Gennaretti, M., Masarati, P., Quaranta, G., and Dieterich, O., "Aeroelastic and Biody-

namic Modeling for Stability Analysis of Rotorcraft-Pilot Coupling Phenomena," Proceeding of the 34th European Rotorcraft Forum, September 16–19 2008.

[34]Gennaretti, M., Serafini, J., Masarati, P., and Quaranta, G., "Effects of Biodynamic Feedthrough in Rotorcraft-Pilot Coupling: Collective Bounce Case," *J. of Guidance, Control, and Dynamics*, Vol. 36, (6), doi:10.2514/1.61355, 2013, pp. 1709–1721.

[35]Quaranta, G., Muscarello, V., and Masarati, P., "Lead-Lag Damper Robustness Analysis for Helicopter Ground Resonance," *J. of Guidance, Control, and Dynamics*, Vol. 36, (4), doi:10.2514/1.57188, July 2013, pp. 1150–1161.

[36]Quaranta, G., Tamer, A., Muscarello, V., Masarati, P., Gennaretti, M., Serafini, J., and Colella, M. M., "Rotorcraft Aeroelastic Stability Using Robust Analysis," *CEAS Aeronaut. J.*, Vol. 5, (1), doi:10.1007/s13272-013-0082-z, March 2014, pp. 29–39.

[37]Desoer, C. and Wang, Y., "On the generalized Nyquist stability criterion," *IEEE Transactions on Automatic Control*, Vol. 25, (2), 1980, pp. 187–196.

[38]Friedland, B., *Control system design: an introduction to state-space methods*, McGraw-Hill, New York, NY, 1987.
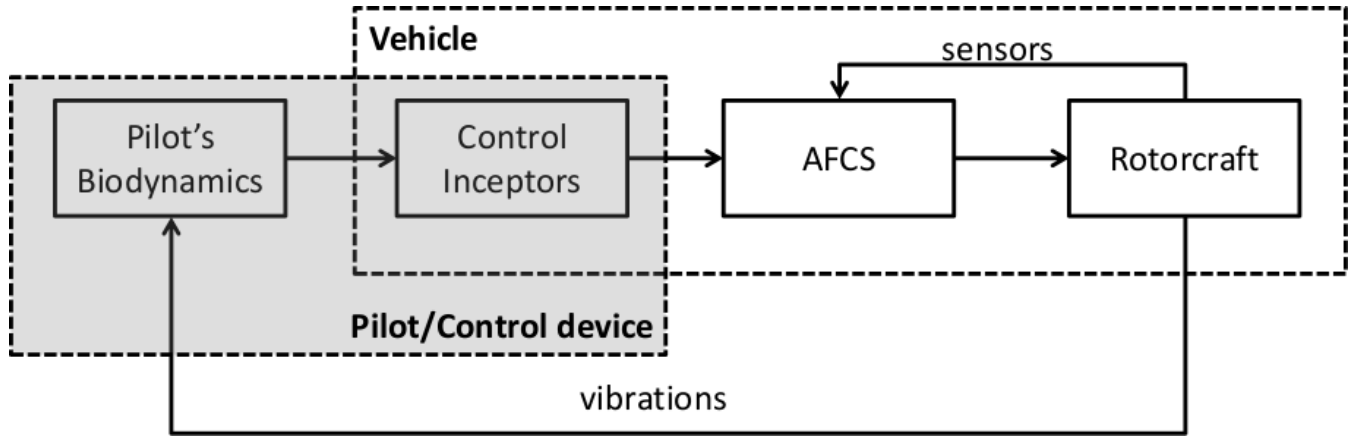
Fig. 1 Block diagram of pilot-vehicle interaction.
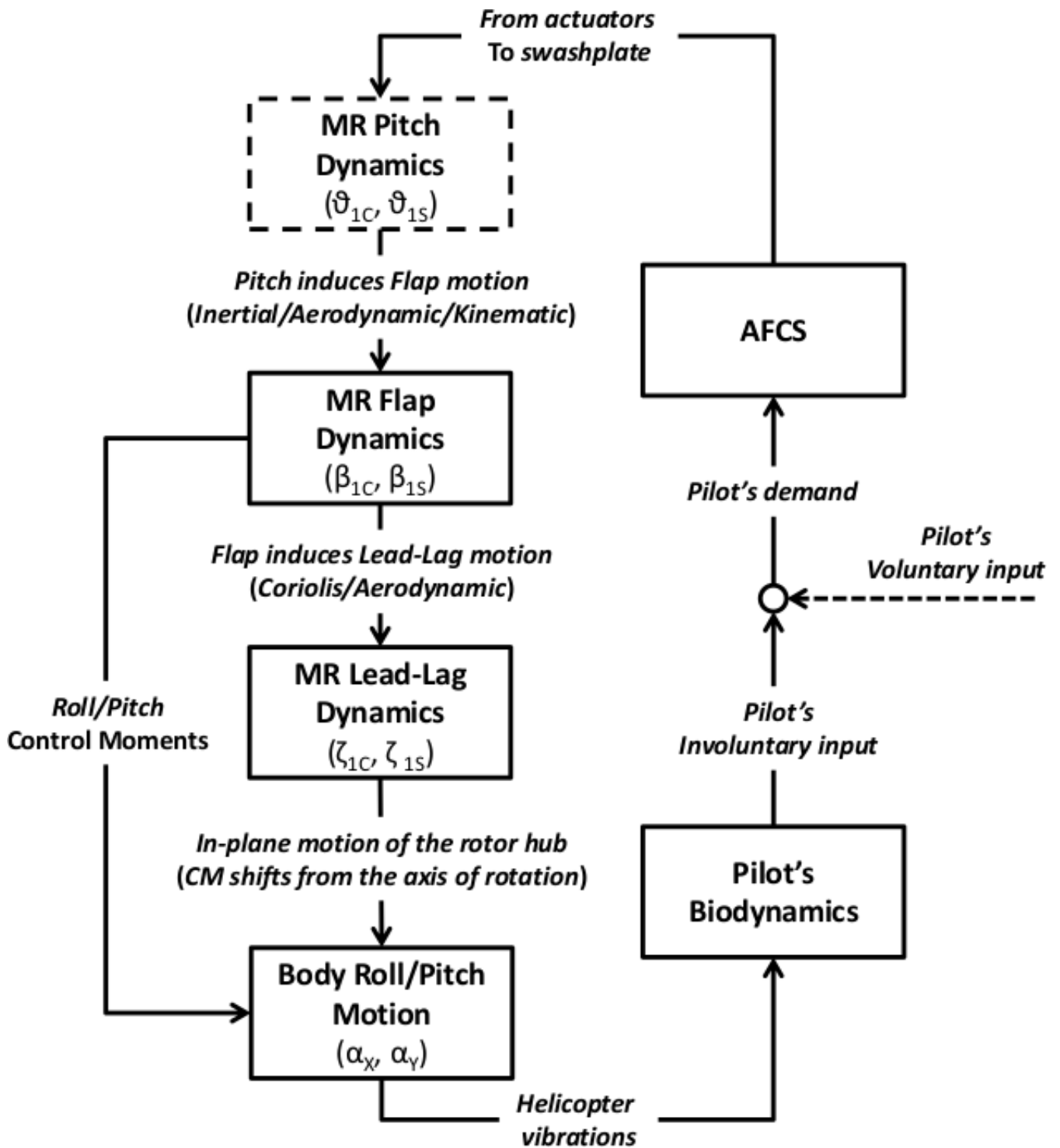
Fig. 2 The lateral PAO mechanism of instability.
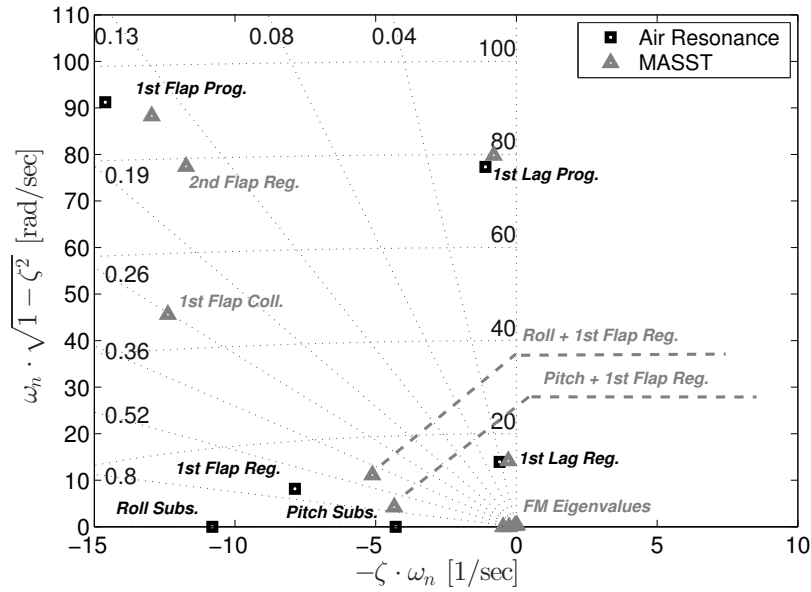
(a) Overall stability map.
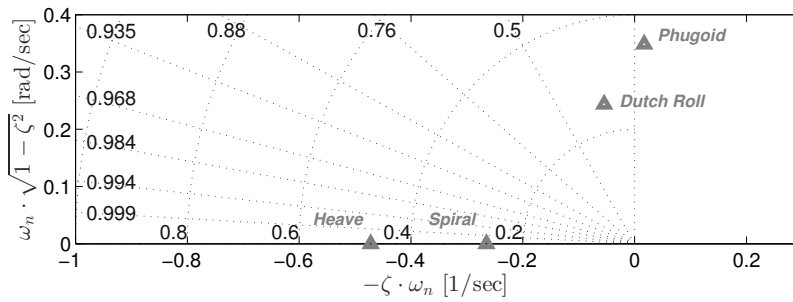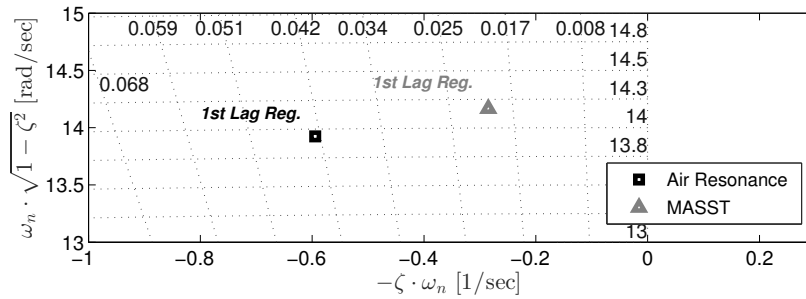
(b) Zoom: 1st lag reg. (Top) - Detail of FM roots (Bottom).

Fig. 3 Eigenvalues: Air Resonance model vs MASST model.
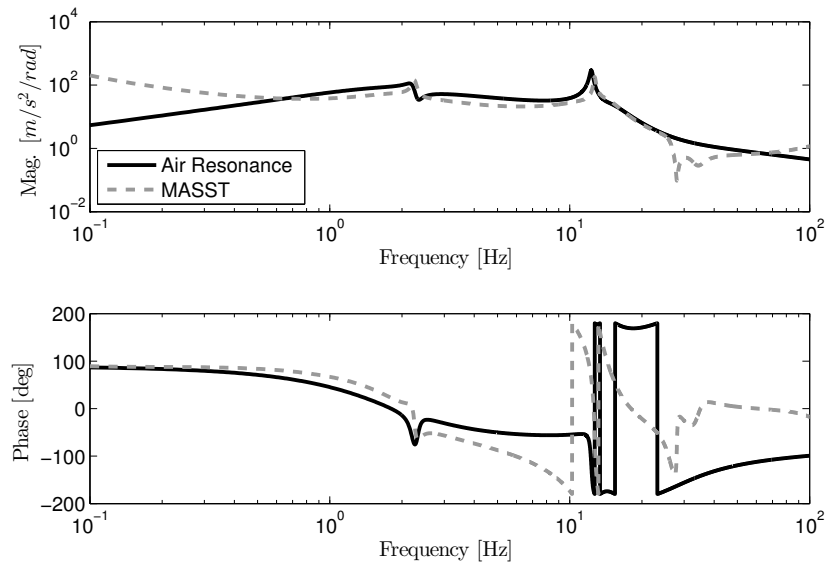
Fig. 4 Bode plot of H_{YC}: Air Resonance model vs MASST model.
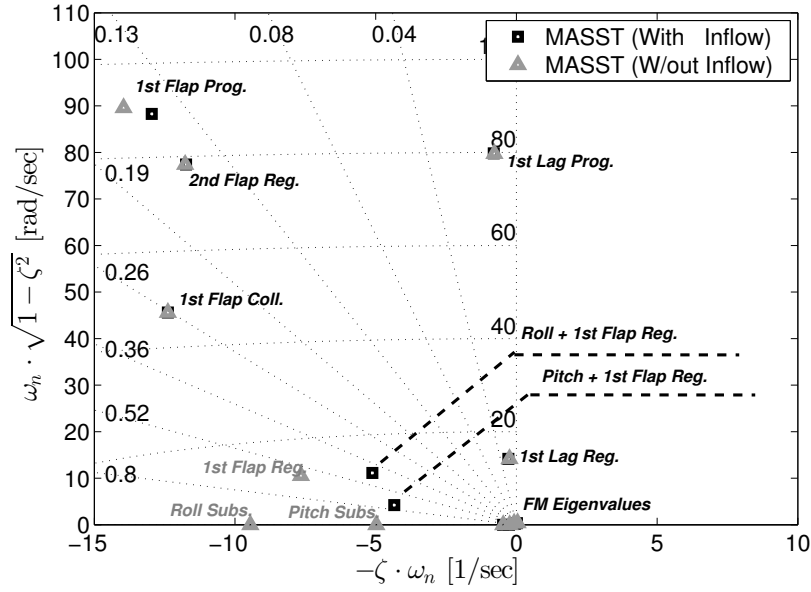
(a) Eigenvalues.
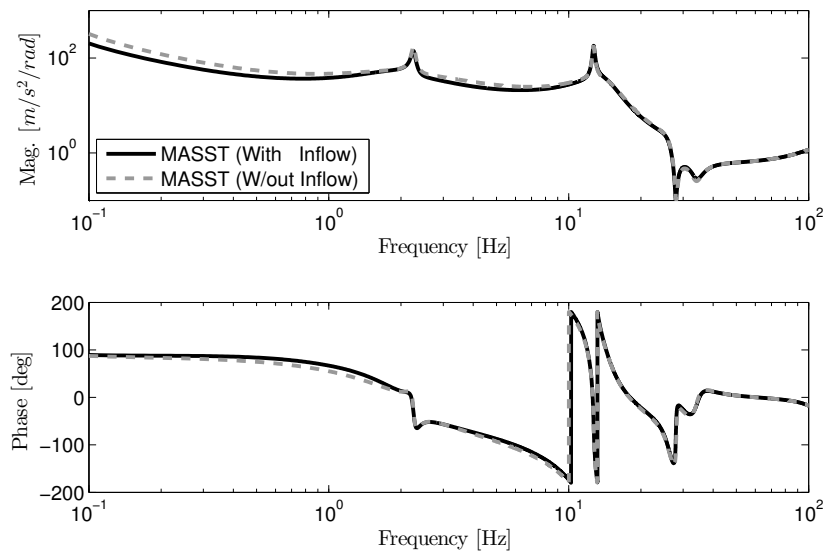
(b) Bode plot of $H_{YC}(s, \mathbf{p})$.

Fig. 5 Effect of inflow states on the BO105 dynamics.
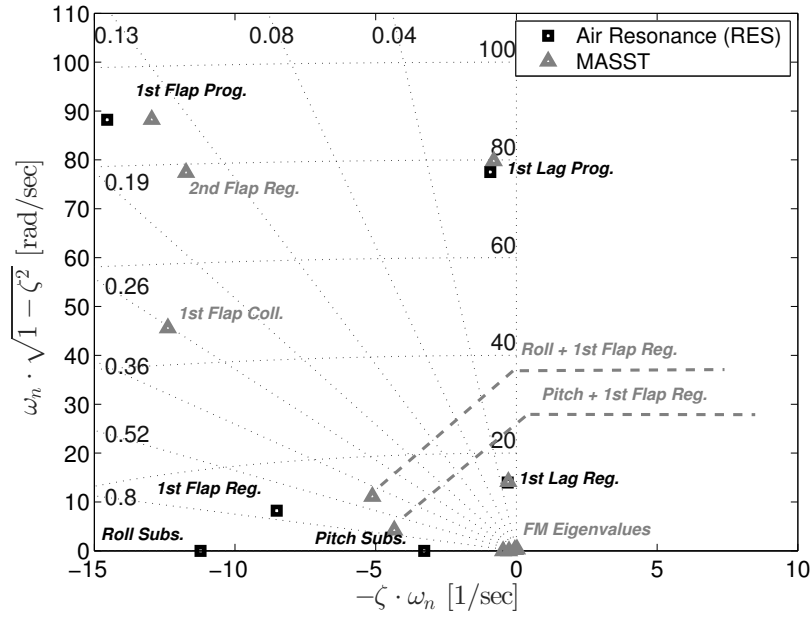
(a) Overall stability map.
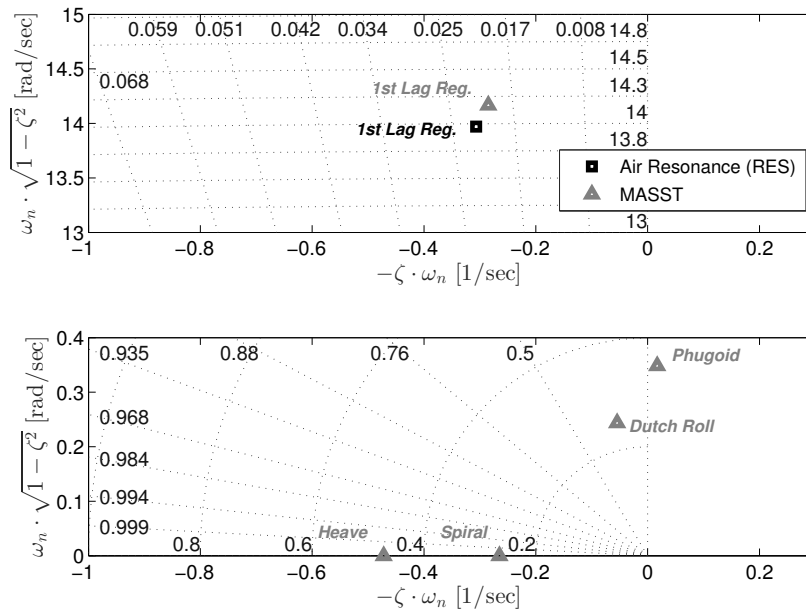
(b) Zoom: 1st lag reg. (Top) - Detail of FM roots (Bottom).

Fig. 6 Eigenvalues: Air Resonance model with residualized pitch dynamics vs MASST model.
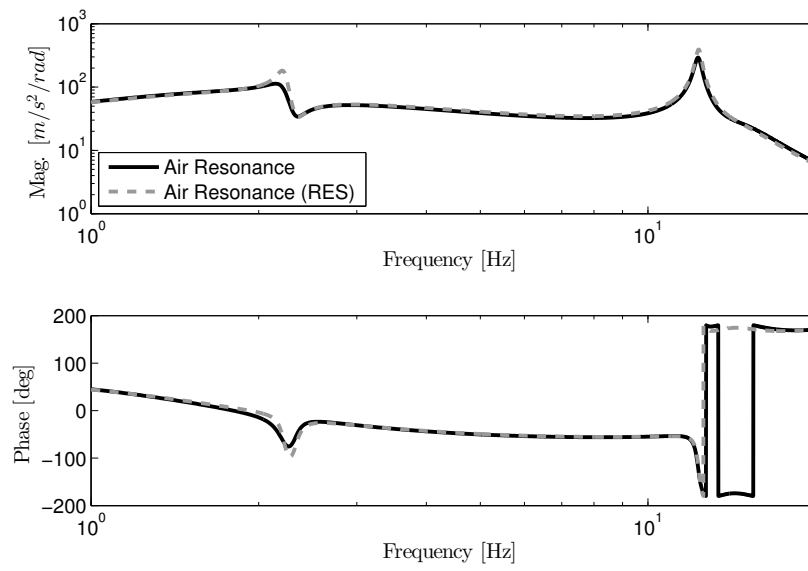
Fig. 7 Bode plot of H_{YC}: effect of residualized pitch dynamics.
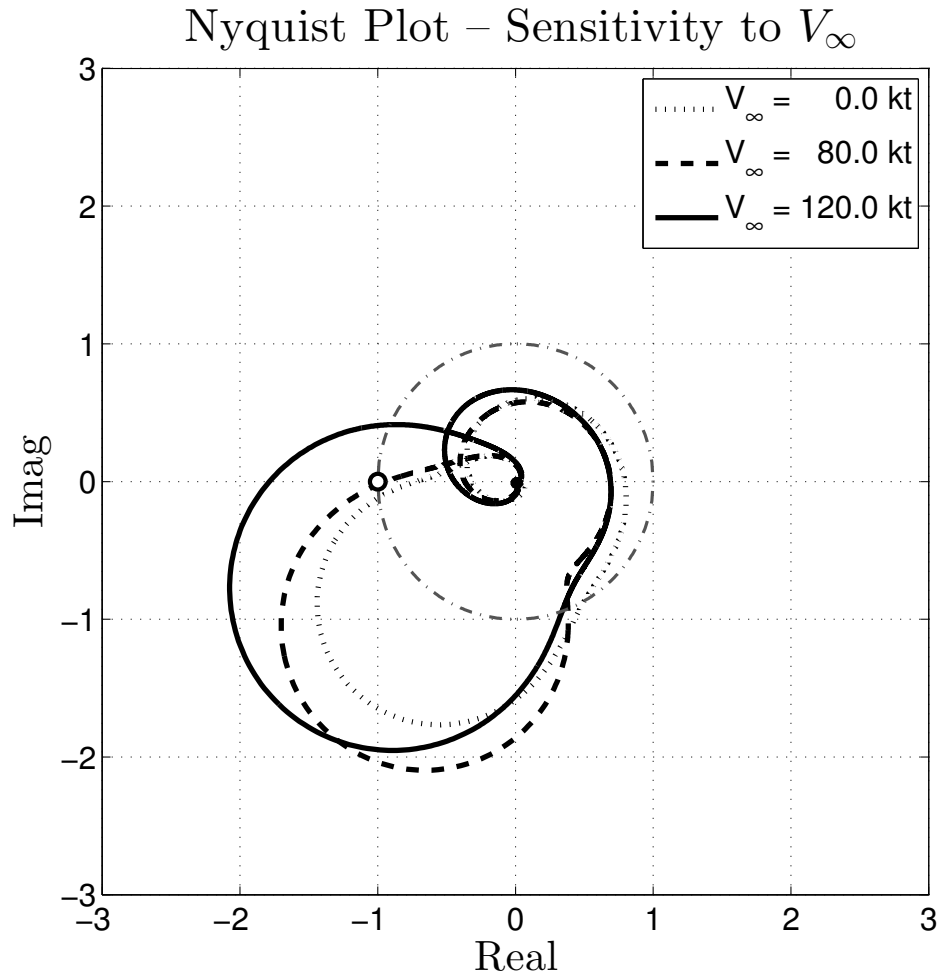
Fig. 8 Nyquist plot of the LTF: $G_Y = 2.5$; $\tau_Y = 140$ ms – Test Pilot #1, SLS.

Stability Map – Sensitivity to Pilot

(a) Stability Map.

Loop Transfer Function – Sensitivity to Pilot

(b) Bode plot of $H_{\mathrm{nom}}(s, \mathbf{p})$.
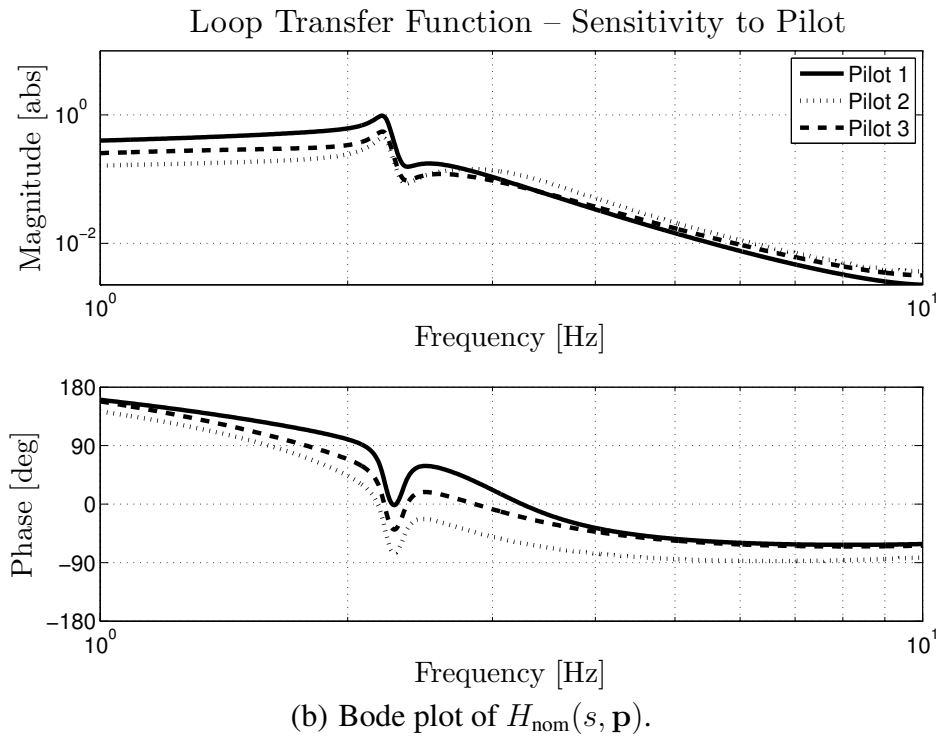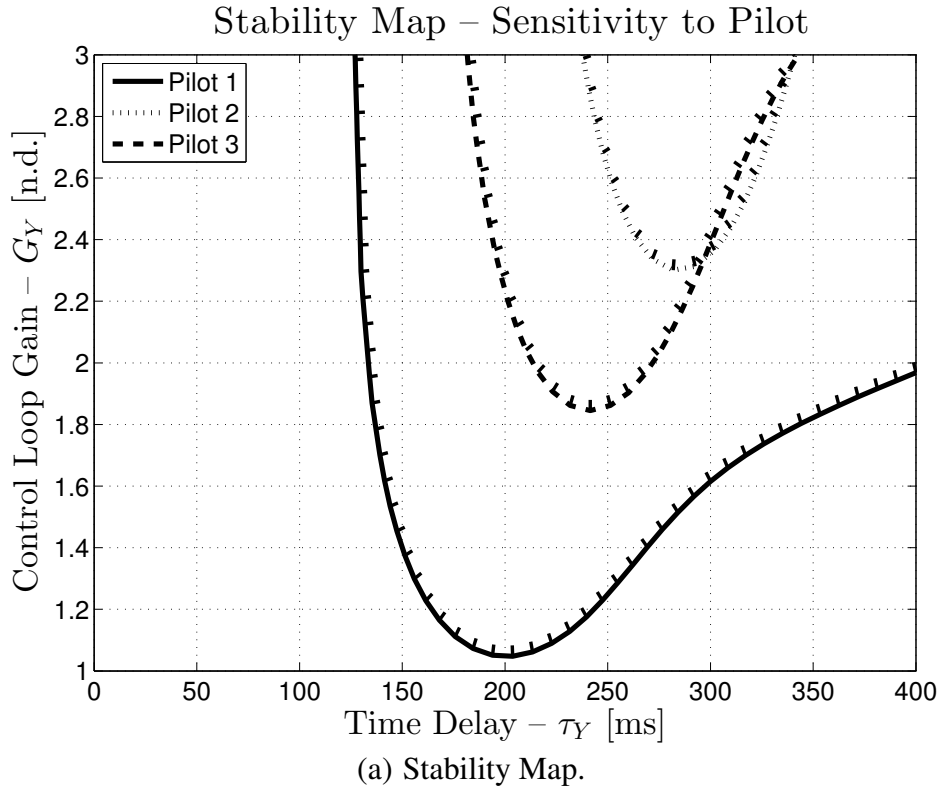
Fig. 9 Sensitivity to pilot's biodynamic feedthrough – Hover, SLS.

Stability Map – Sensitivity to I_{xx}

(a) Roll Inertia.

Stability Map – Sensitivity to I_{yy}

(b) Pitch Inertia.
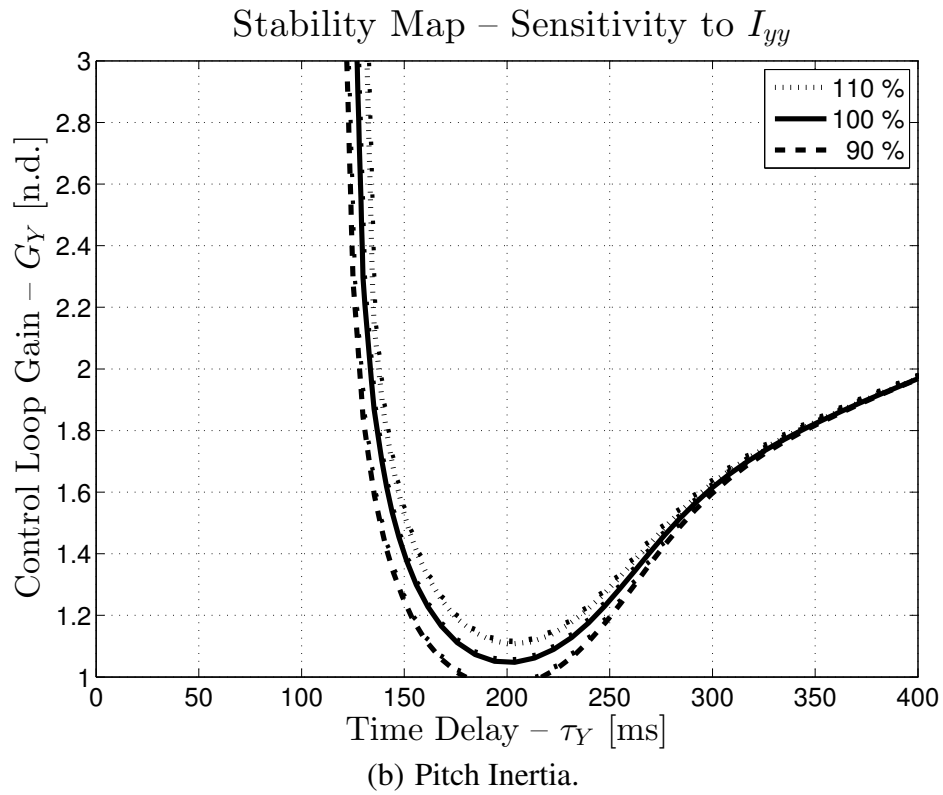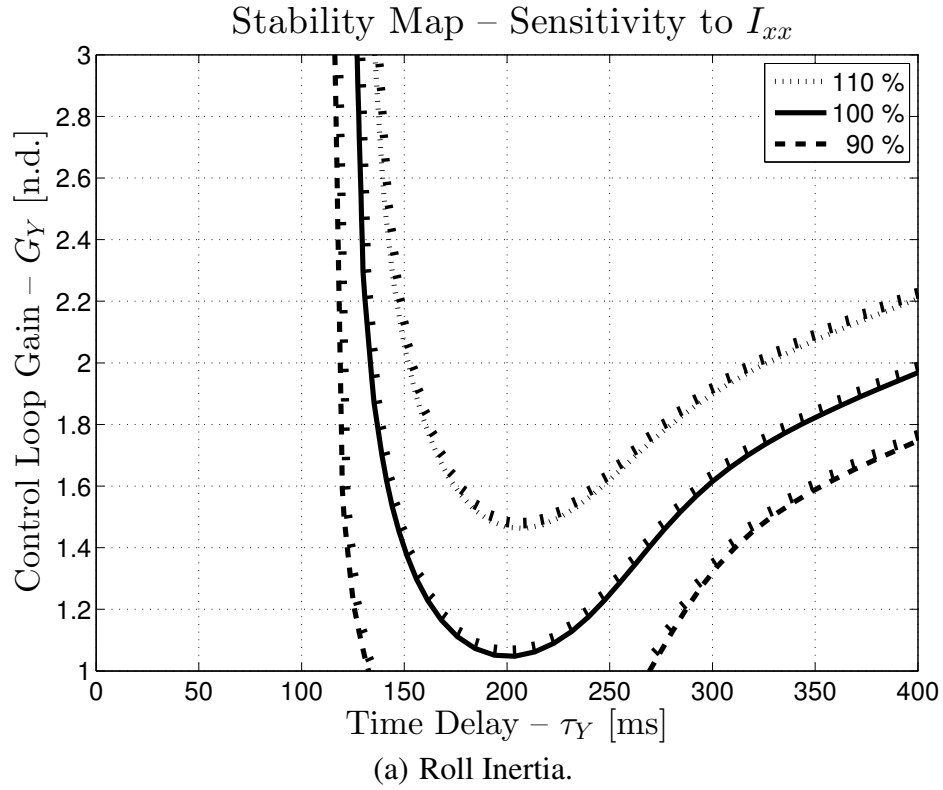
Fig. 10 Sensitivity to rotorcraft inertia – Hover, SLS.

(a) Stability Map.

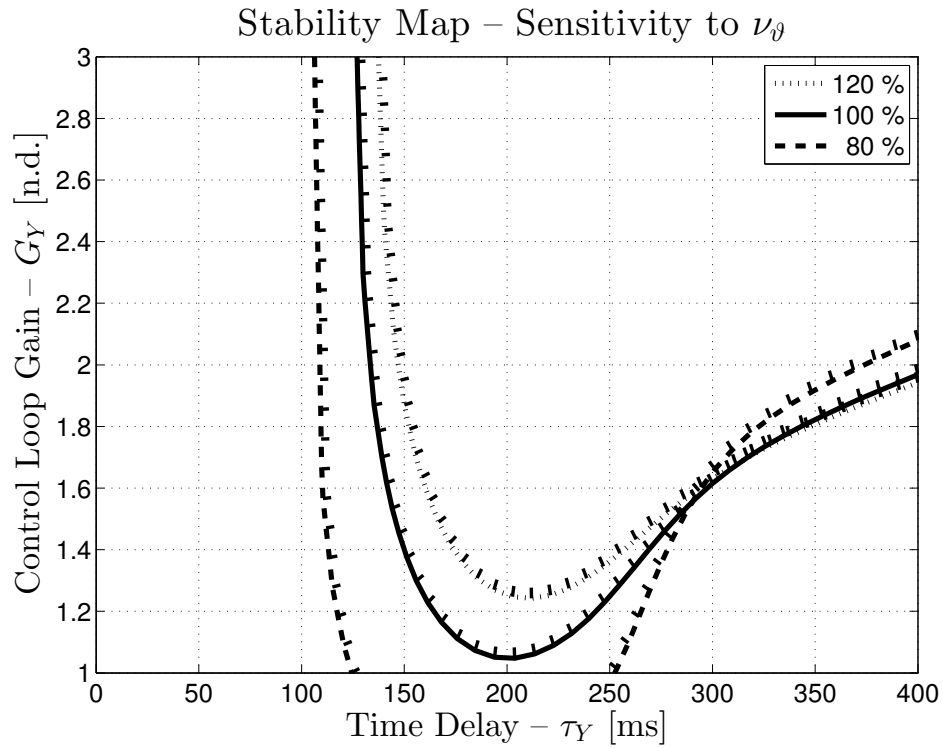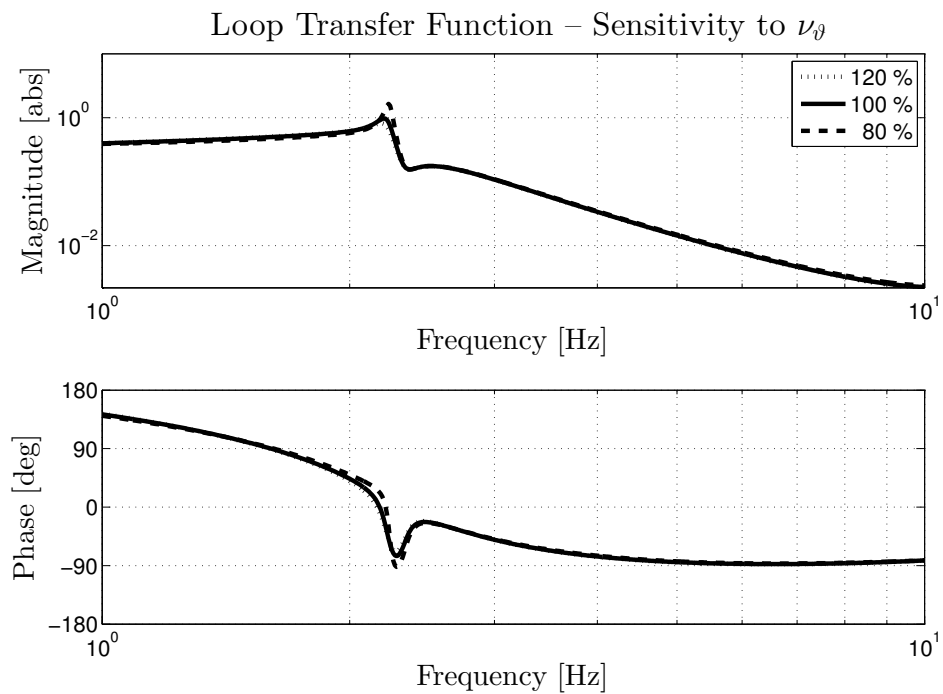
(b) Bode plot of $H_{\mathrm{nom}}(s, \mathbf{p})$.
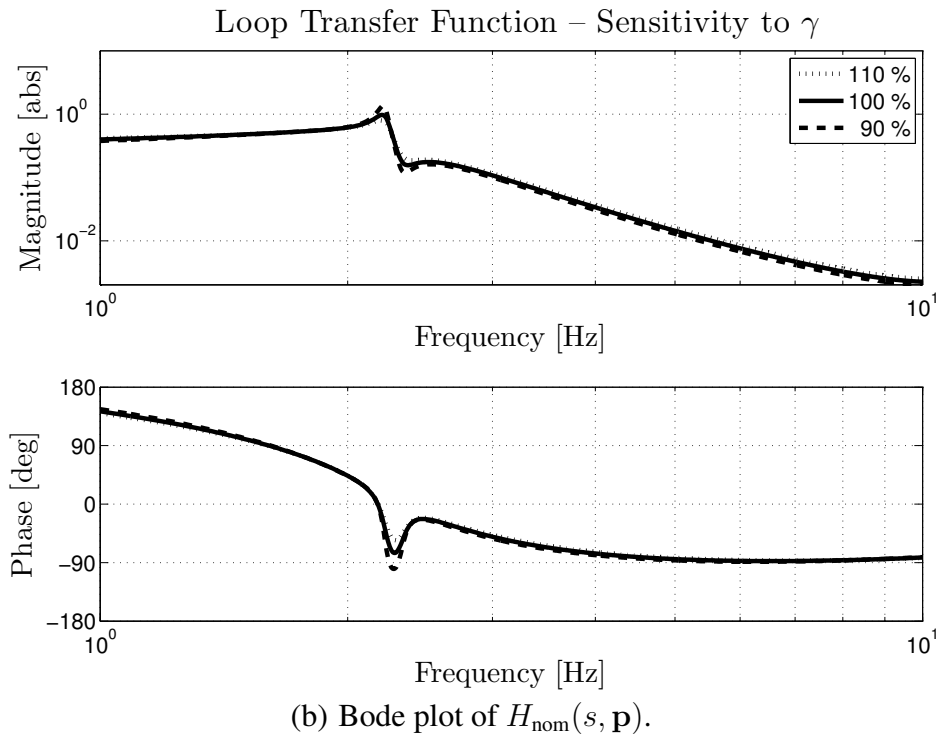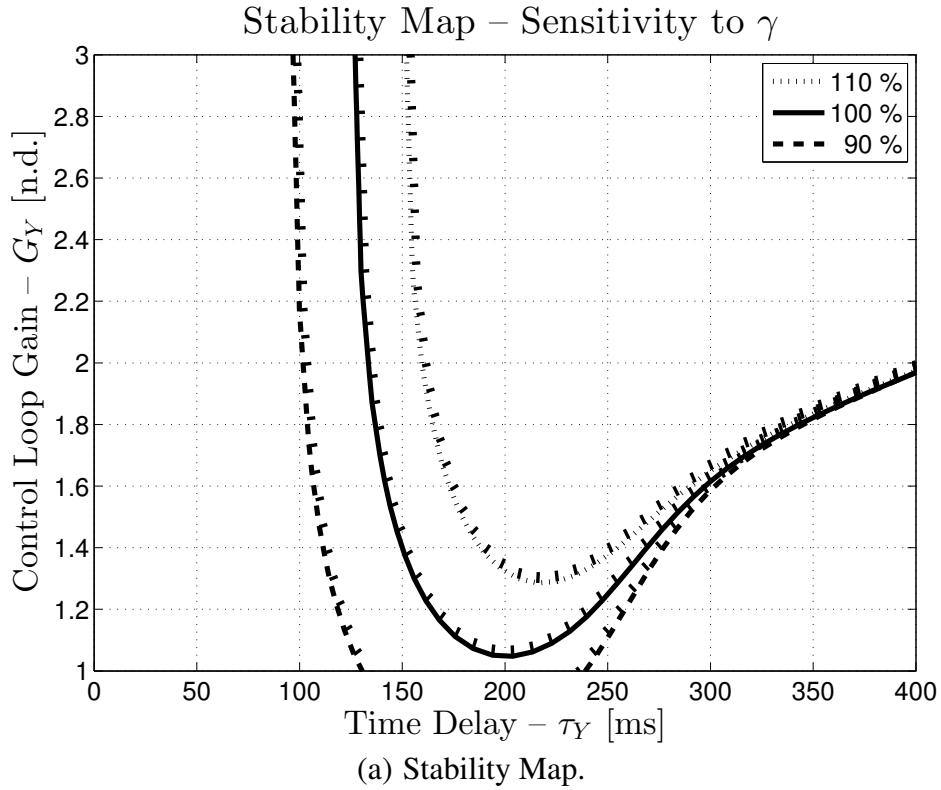
Fig. 11 Sensitivity to Lock number – Hover, SLS.

(a) Stability Map.

(b) Bode plot of $H_{\text{nom}}(s, \mathbf{p})$.
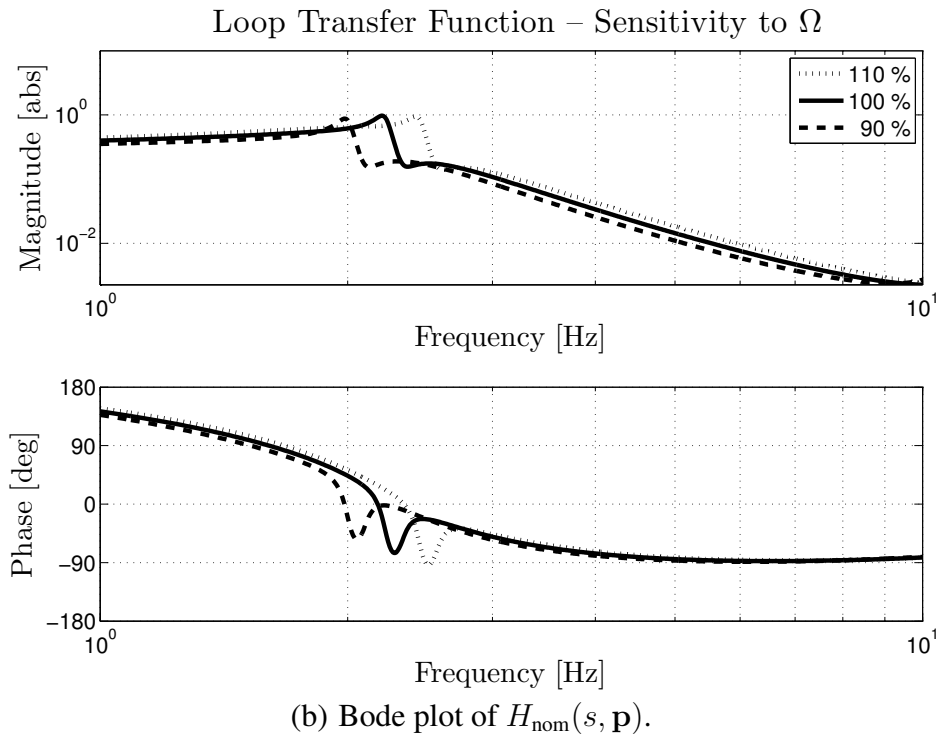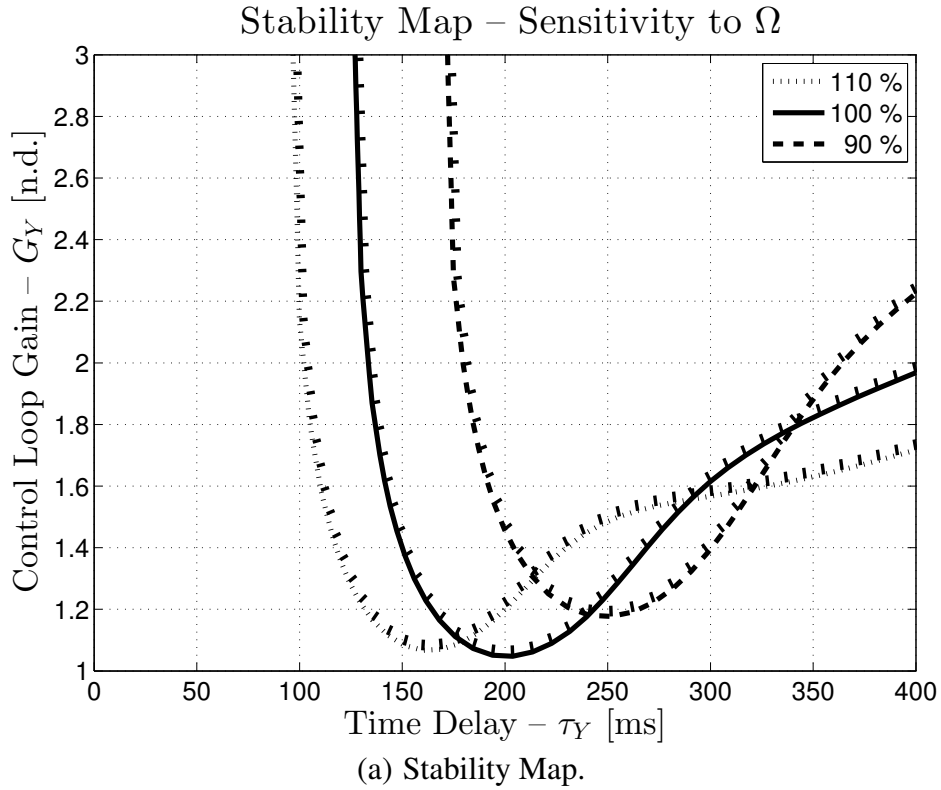
Fig. 12 Sensitivity to rotor speed – Hover, SLS.

(a) Stability Map.

(b) Bode plot of $H_{nom}(s, \mathbf{p})$.
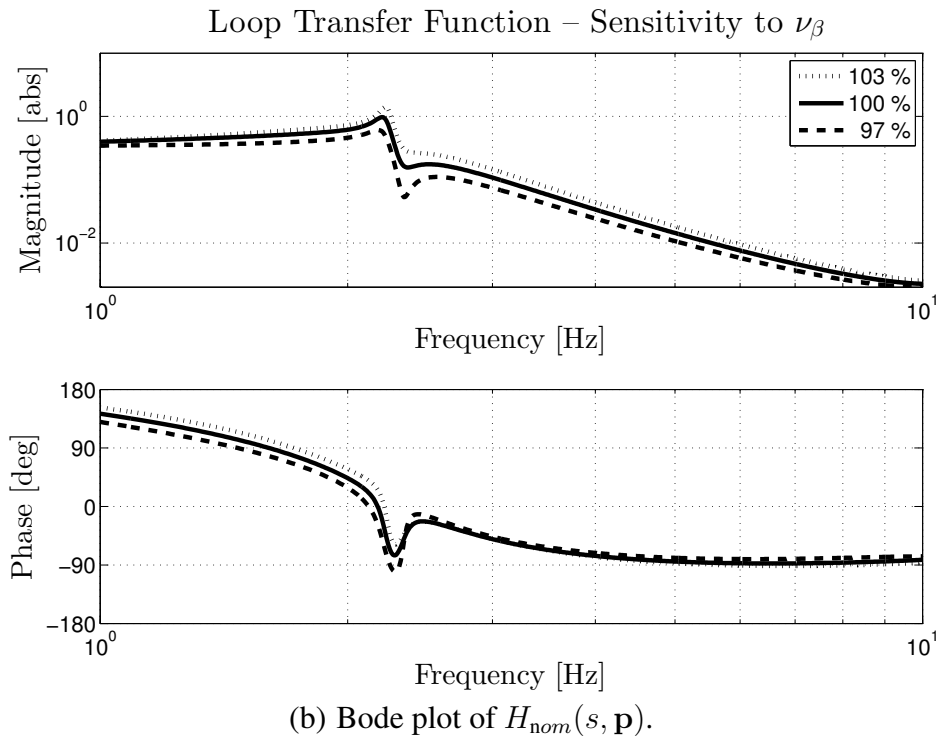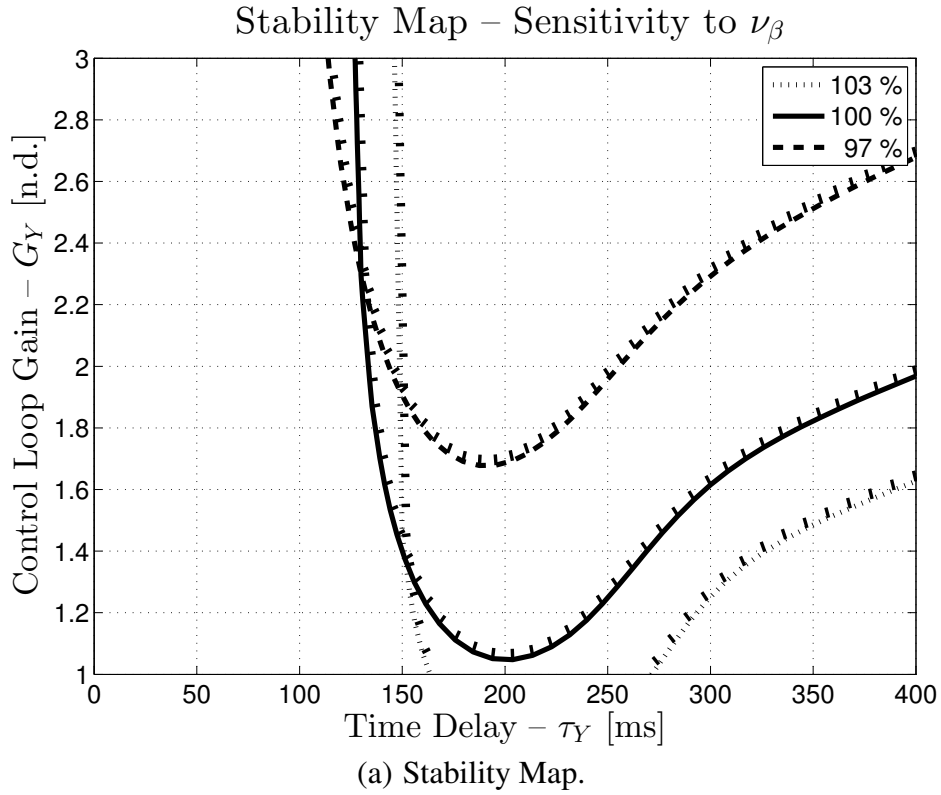
Fig. 13 Sensitivity to flap frequency – Hover, SLS.

(a) Stability Map.

(b) Bode plot of $H_{\text{nom}}(s, \mathbf{p})$.
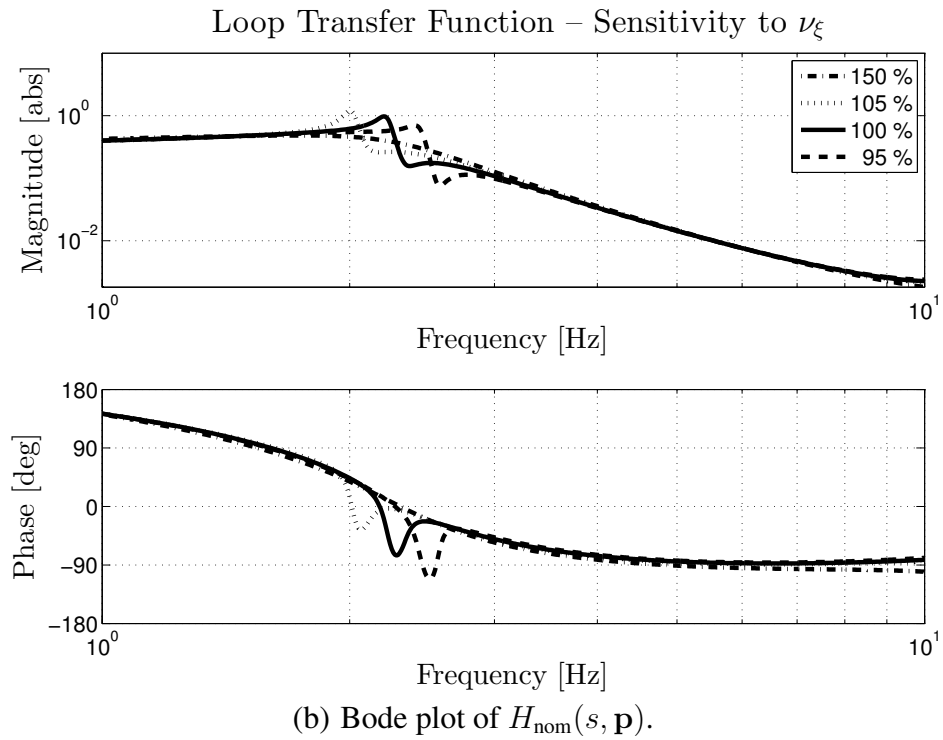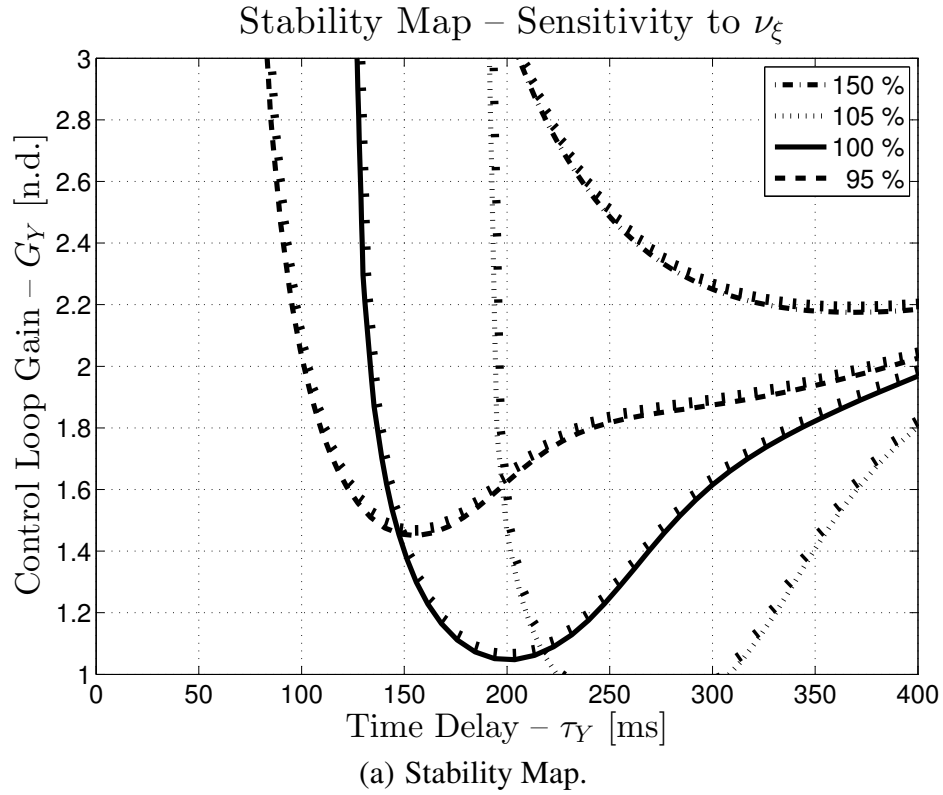
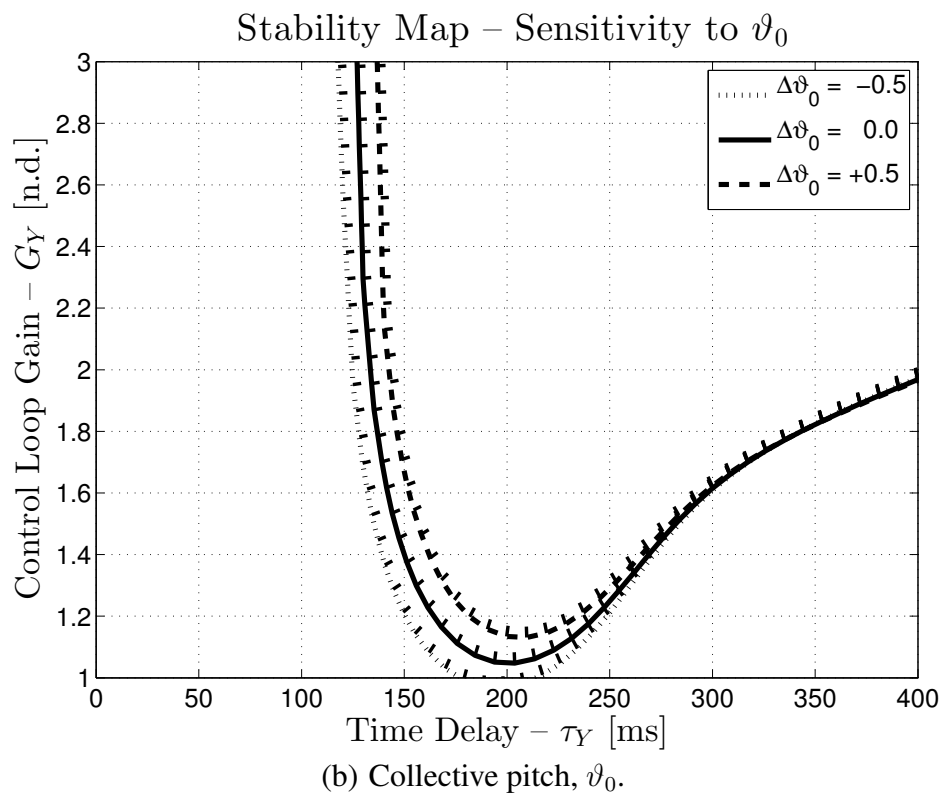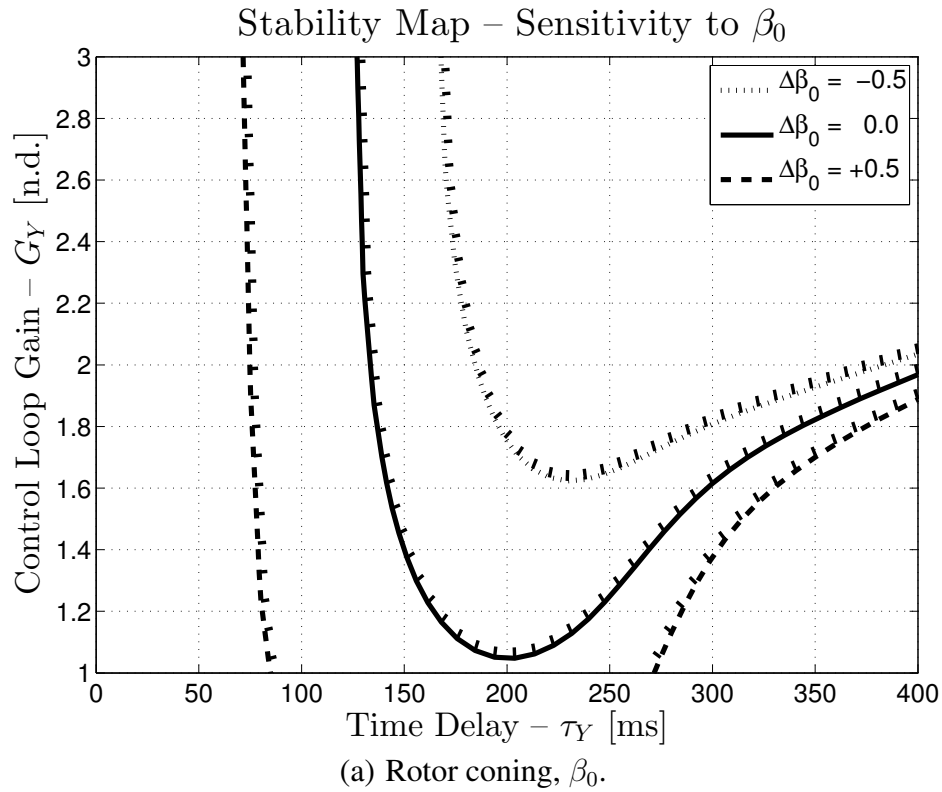**Fig. 14** Sensitivity to lead-lag frequency – Hover, SLS.

Stability Map – Sensitivity to ν_ϑ

(a) Stability Map.

Loop Transfer Function – Sensitivity to ν_ϑ

(b) Bode plot of $H_{\mathrm{nom}}(s, \mathbf{p})$.

Fig. 15 Sensitivity to pitch frequency – Hover, SLS.

(a) Rotor coning, β_0.

(b) Collective pitch, ϑ_0.
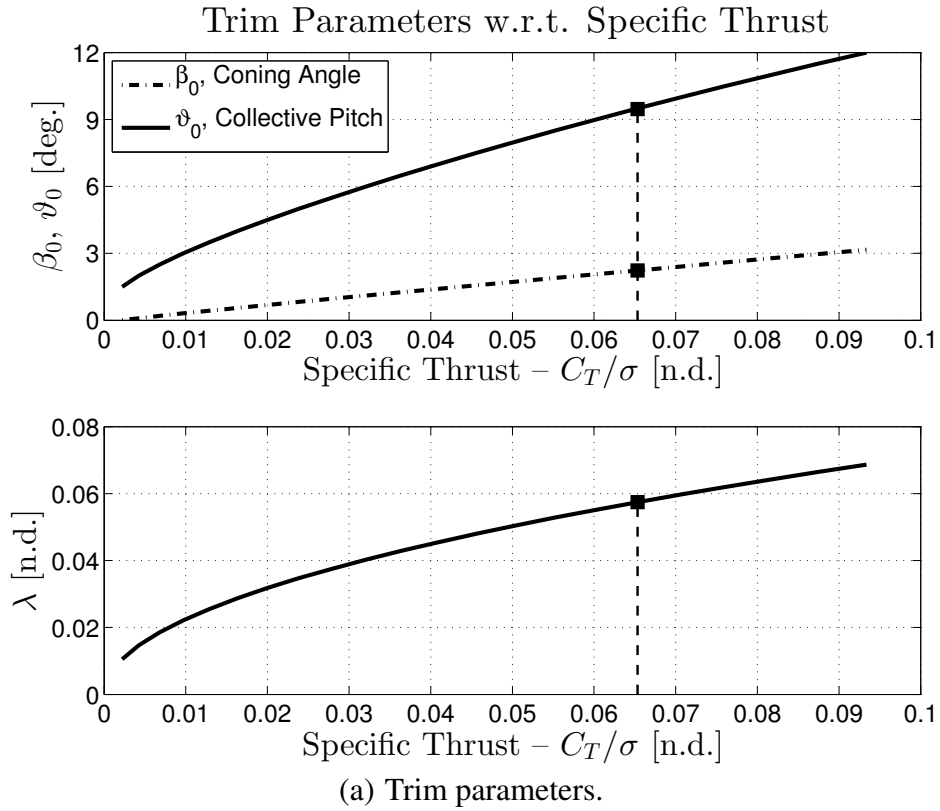
Fig. 16 Sensitivity to rotor trim angles – Hover, SLS.

(a) Trim parameters.
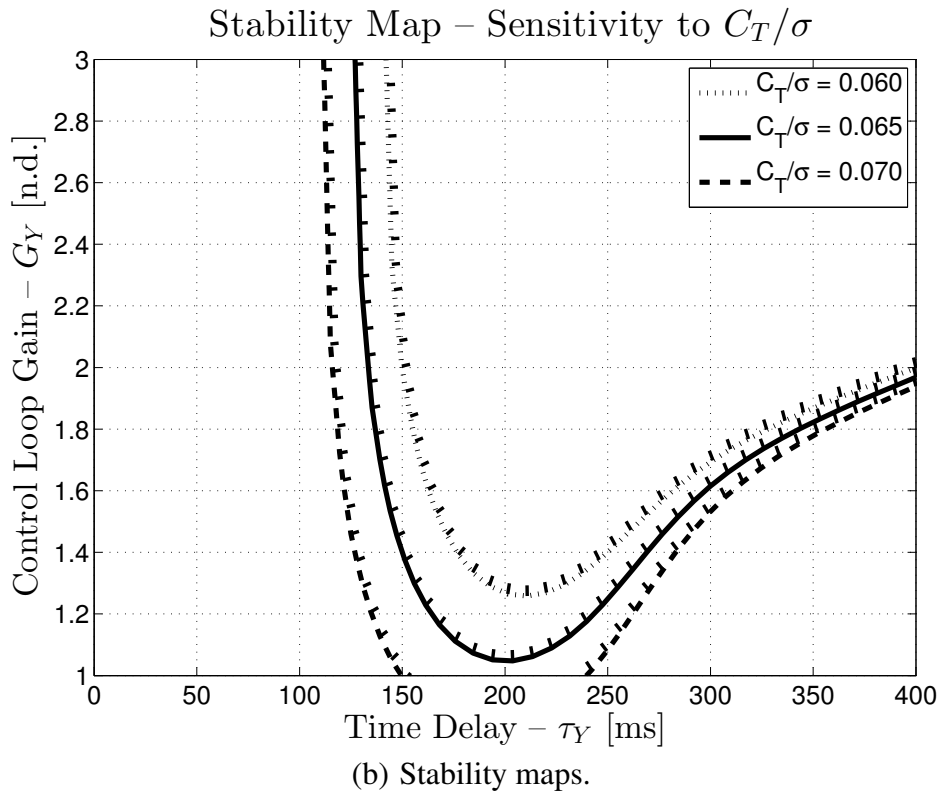
(b) Stability maps.

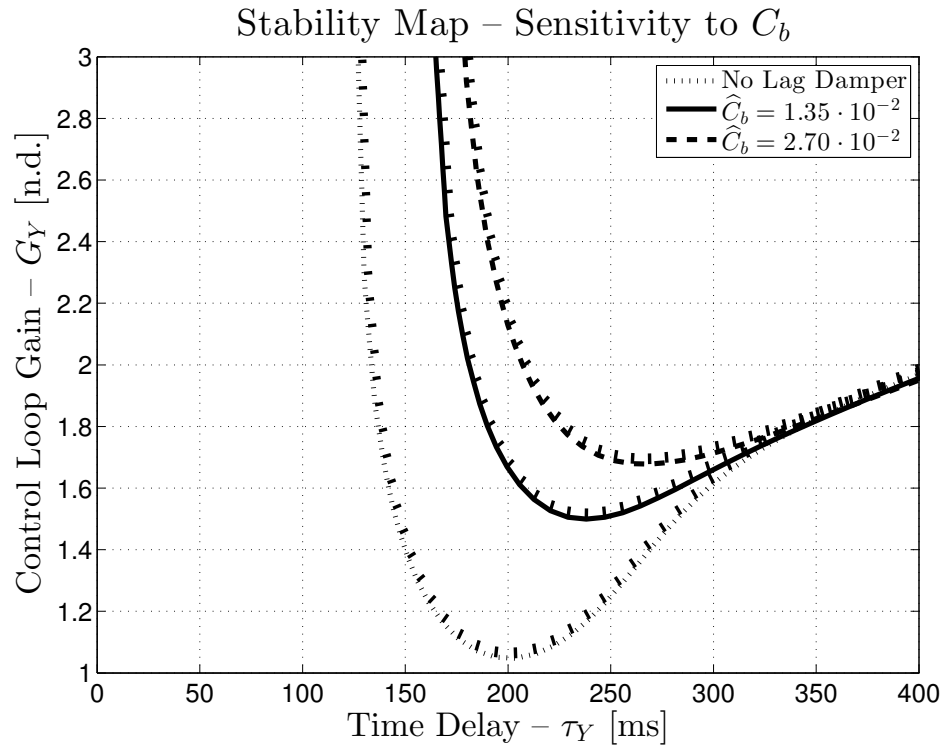**Fig. 17** Sensitivity to specific rotor thrust C_T/σ – Hover, SLS.
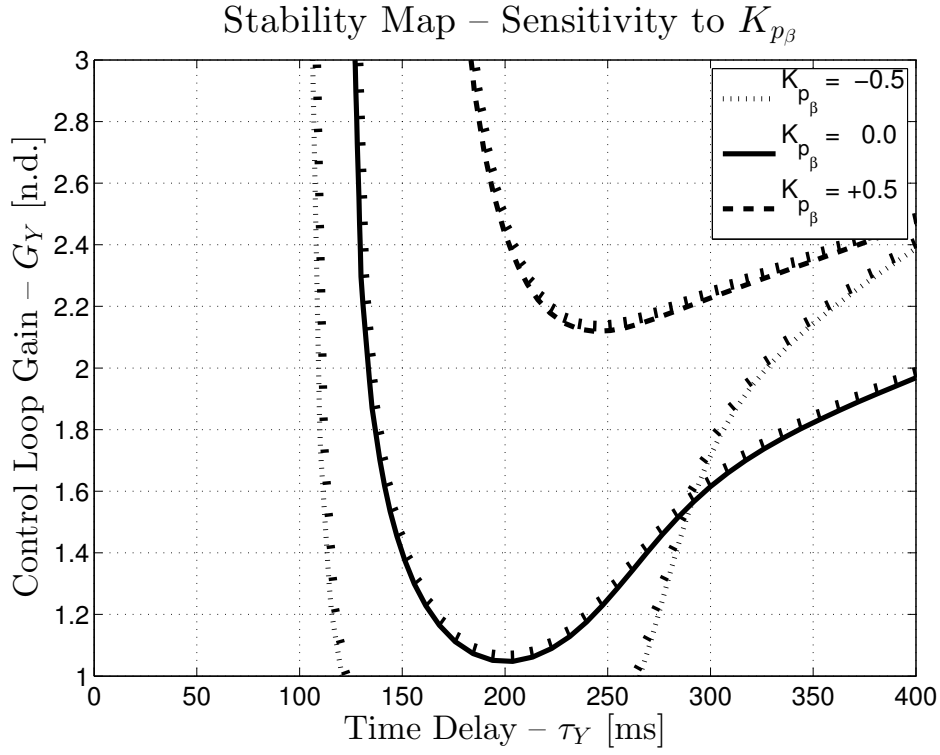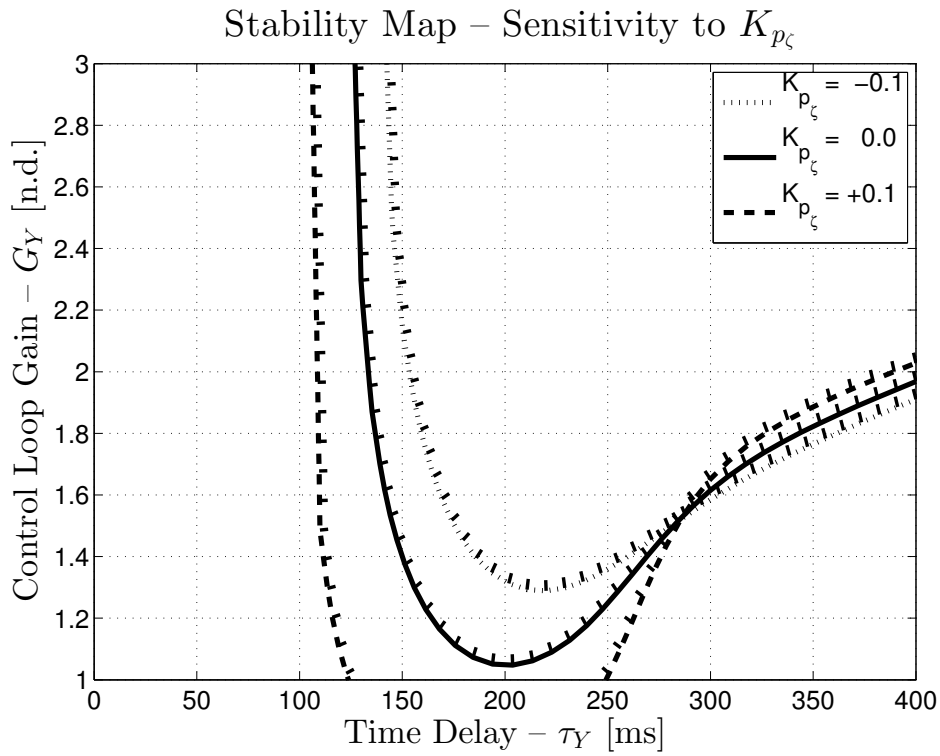
Fig. 18 Stability map of the LTF with different lead-lag damping – Hover, SLS.

(a) Pitch-Flap coupling, K_{p_β}.

(b) Pitch-Lag coupling, K_{p_ζ}.

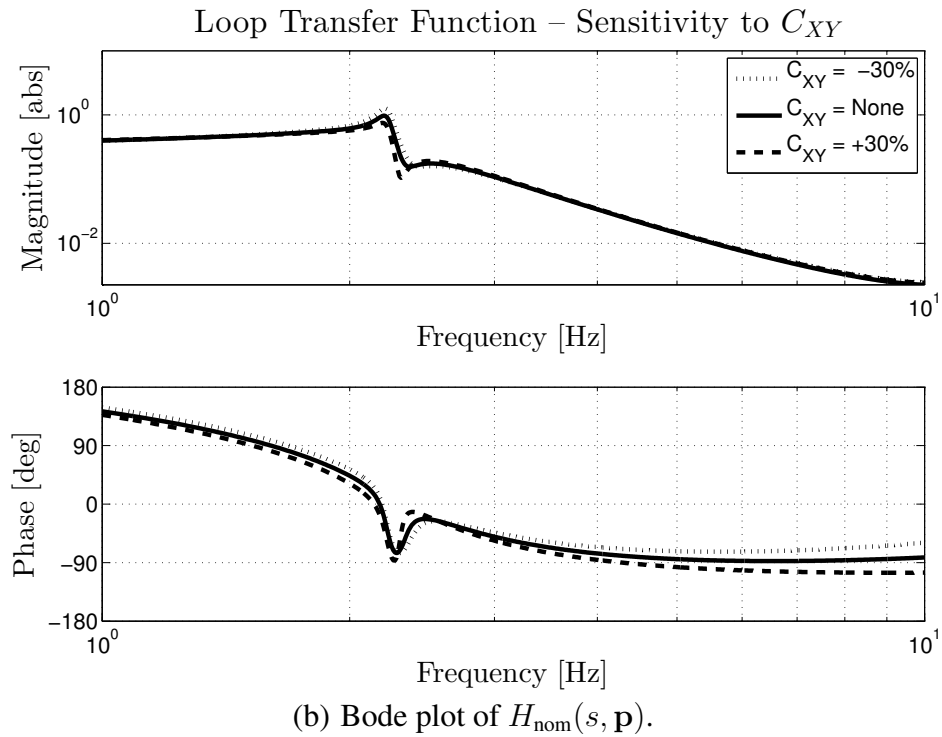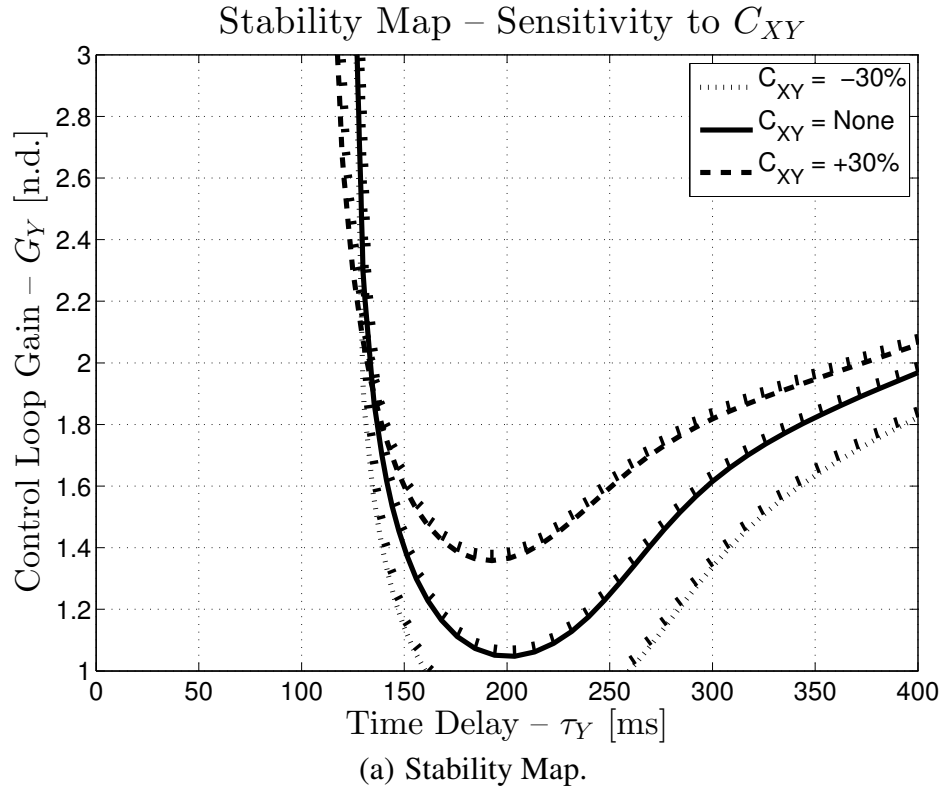**Fig. 19** Stability maps of the LTF with different blade kinematic couplings – Hover, SLS.

(a) Stability Map.

(b) Bode plot of $H_{\text{nom}}(s, \mathbf{p})$.

Fig. 20 Effect of longitudinal cyclic stick BDFT on Roll/Lateral PAO – Hover, SLS.

Table 1.   Pilot/Lateral Stick dynamic properties.

	Pilot #1	Pilot #2	Pilot #3	Units
μ_P	216.26	88.67	83.88	%/g
T_z	0.02	0.05	0.03	s
T_p	0.51	0.49	0.26	s
ξ	26.87	23.11	39.66	%
ω_n	14.12	19.05	16.14	rad/s

Table 2. Eigenvalues of the 6-DOF Air Resonance model – Hover, SLS.

Mode	Eigen. [rad/s]	Freq. [Hz]	Damp. [%]	Mode Shape
1	-4.2916	–	–	Pitch Subsidence
2	-10.8063	–	–	Roll Subsidence
3	$-7.8697 \pm i\, 8.1586$	1.298	69.42	Flap Regressive
4	$-0.5946 \pm i13.9244$	2.216	4.27	Lag Regressive
5	$-1.1026 \pm i77.3165$	12.305	1.43	Lag Progressive
6	$-14.6088 \pm i91.2162$	14.517	15.81	Flap Progressive

Table 3. Eigenvalues of the 6-DOF Air Resonance model with residualized pitch dynamics – Hover, SLS.

Mode	Eigen. [rad/s]	Freq. [Hz]	Damp. [%]	Mode Shape
1	-3.2759	–	–	Pitch Subsidence
2	-11.2243	–	–	Roll Subsidence
3	$-8.5157 \pm i\, 8.2144$	1.307	71.97	Flap Regressive
4	$-0.3068 \pm i 13.9703$	2.223	2.19	Lag Regressive
5	$-0.9277 \pm i 77.5087$	12.336	1.20	Lag Progressive
6	$-14.5416 \pm i 88.2133$	14.039	16.26	Flap Progressive